Available online at www.sciencedirect.com
SCIENCE DIRECT®
International Journal of Thermal Sciences 44 (2005) 623–643
International Journal of Thermal Sciences
www.elsevier.com/locate/ijts

Some recent advances in finite volume approach and their applications in the study of heat transfer enhancement ☆

W.Q. Tao *, Y.L. He, Z.Y. Li, Z.G. Qu

State Key Laboratory of Multiphase Flow in Power Engineering, School of Energy & Power Engineering, Xi'an Jiaotong University, Xi'an, Shaanxi 710049, China

Received 10 August 2004; received in revised form 21 January 2005; accepted 2 February 2005

Available online 12 April 2005

Abstract

In the finite volume approach for incompressible flow and heat transfer, the discretization of the convection term and the treatment of the coupling between velocity and pressure are the two major issues affecting solution stability, accuracy and convergence rate. In this review paper, some recent advances made in the CFD/NHT & Enhanced Heat Transfer Center of Xi'an Jiaotong University, China, are presented and their applications in the study of heat transfer enhancement are also briefly summarized.

Keywords: Numerical heat transfer; Stability of discretized convective term; Convective boundedness; Coupling between velocity and pressure; Enhancement of heat transfer; Field synergy principle

1. Advances in the study of stability of discretized convective term

1.1. How to judge a discretized convective term stable or conditionally stable

The convective term in the convection–diffusion equation, which is a partial derivative of first-order, can be discretized either by finite difference method or by finite volume method. For whatever method, the final result is an algebraic expression relating the values of field variables at several neighboring grid points. A very simple but useful criterion for judging whether the scheme is absolutely stable or conditionally stable is proposed in [1]. If the expression contains a value from the downstream stream grid point, the scheme will violate the transportive property and hence must be only conditionally stable. To get the critical Peclet number a very simple but useful principle(rule), called sign preservation principle, was proposed in [1]. By the critical Peclet number we mean the value of $\rho u \delta x/\Gamma$ beyond which a numerical solution will lead to oscillating results. The implementation procedure of the sign preservation rule is now briefly introduced as follows.

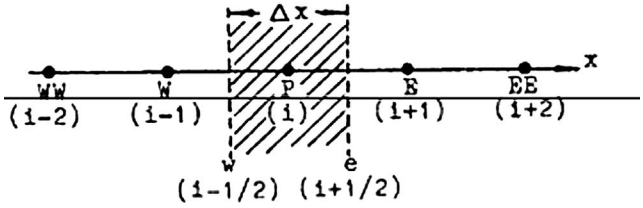

Fig. 1. 1-D uniform grid system.

First we discretize the 1-D model equation on a uniform grid system shown in Fig. 1

$$\rho\left(\frac{\partial\phi}{\partial t}+u\frac{\partial\phi}{\partial x}\right)=\Gamma\frac{\partial^2\phi}{\partial x^2} \tag{1}$$

by an explicit finite difference form into which the examined finite difference scheme is incorporated for the convective

☆ A preliminary version of this paper was presented at CHT-04; An ICHMT International Symposium on Advances in Computational Heat Transfer, April 2004, G. de Vahl Davis and E. Leonardi (Eds.), CD-ROM Proceedings, ISBN 1-5670-174-2, Begell House, New York, 2004.

* Corresponding author.
E-mail address: wqtao@mail.xjtu.edu.cn (W.Q. Tao).

1290-0729/$ – see front matter © 2005 Elsevier SAS. All rights reserved.
doi:10.1016/j.ijthermalsci.2005.02.007

Nomenclature

$a_{E,W,N,S,P}$	coefficients in discretization equation
A	surface area
b	source term in discretization equation
d	coefficient in velocity correction equation
P_Δ	critical grid Peclet umber
p	pressure
p'	pressure correction
p^*	assumed or previous pressure
t	time
T	temperature
$\vec{U}$	velocity vector
u, v	u-component, v-component of velocity
u', v'	u and v velocity correction term
x	x-coordinate
y	y-coordinate

Greek symbols

α	relaxation factor
β	second relaxation factor
δ	effect of disturbance
∇T	temperature gradient
δx	step length in x-direction
δy	step length in y-direction
ε	disturbance
ϕ	general variable
Γ	nominal diffusion coefficient
λ	thermal conductivity
μ	dynamic viscosity
θ	synergy angle
ρ	fluid density

Subscripts

C	central
D	downstream
e	east
f	interface
U	upstream
w	west

term and the central difference for the diffusion term. Assume that a steady-state solution $\phi_i = 0$ exists for all i. Then at an arbitrary time step n a disturbance $\varepsilon_i = \delta$ is introduced at single grid point i with $\varepsilon = 0$ at all other grids. The effect of this disturbance is then determined by the finite difference equation at time step $(n+1)$ and grid points $(i \pm 1)$. In order that a finite difference solution be physically realistic, it is required that the sign of the resulting disturbances at grid points $(i \pm 1)$ be the same as the disturbance imposed at grid i at time step n. The sign preservation requirement sets a limit for the conditions under which the finite difference equation is applicable. Via such analysis we can reveal whether the scheme is absolutely stable, and if not what is its critical Peclet number.

Let us perform such an analysis for TUD. The discretized equation for $u > 0$ reads:

$$\rho\left(\frac{\phi_i^{n+1}-\phi_i^n}{\Delta t}+u\frac{4\phi_{i+1}^n+6\phi_i^n-12\phi_{i-1}^n+2\phi_{i-2}^n}{12\Delta x}\right) = \Gamma\frac{\phi_{i+1}^n-2\phi_i^n+\phi_{i-1}^n}{\Delta x^2} \tag{2}$$

At grid point $(i-1)$ we have

$$\rho\left(\frac{\phi_{i-1}^{n+1}-\phi_{i-1}^n}{\Delta t}+u\frac{4\phi_i^n+6\phi_{i-1}^n-12\phi_{i-2}^n+2\phi_{i-3}^n}{12\Delta x}\right) = \Gamma\frac{\phi_i^n-2\phi_{i-1}^n+\phi_{i-2}^n}{\Delta x^2}$$

We require:

$$\frac{-\frac{1}{3}(\frac{u\Delta t}{\Delta x})\varepsilon_i+(\frac{\Gamma\Delta t}{\rho\Delta x^2})\varepsilon_i}{\varepsilon_i}\geqslant 0$$

This leads to:

$$\frac{\rho u\Delta x}{\Gamma}=P_\Delta\leqslant 3.0$$

It can be shown that at grid $(i+1)$ this requirement is automatically satisfied.

By such analysis we find that FUD and SUD are absolutely stable (i.e., $P_{\Delta\mathrm{cr}}\to\infty$) and obtain following critical Peclet numbers for some widely used conditionally stable schemes:

CD: $P_\Delta = 2.0$

QUICK: $P_\Delta = 8/3$

TUD: $P_\Delta = 3.0$

Fromm: $P_\Delta = 4.0$

It should be noted that the concrete value of the above-mentioned critical Peclet number is with respect to the second-order discretized diffusion term, which is the most often used scheme in engineering computations. If the diffusion term is discretized by other order accuracy scheme, the concrete value of the critical Peclet number may vary, but the quantitative character of the discretized convective term (i.e., conditionally stable or un-conditionally stable) will not change.

1.2. The critical Peclet number obtained by the existing analysis methods is the most severe condition

The existing stability analysis methods for the discretization scheme of a convective term include (1). The positive coefficient method proposed by Patankar [2]; (2) Exact solution analysis method presented by Gresho and

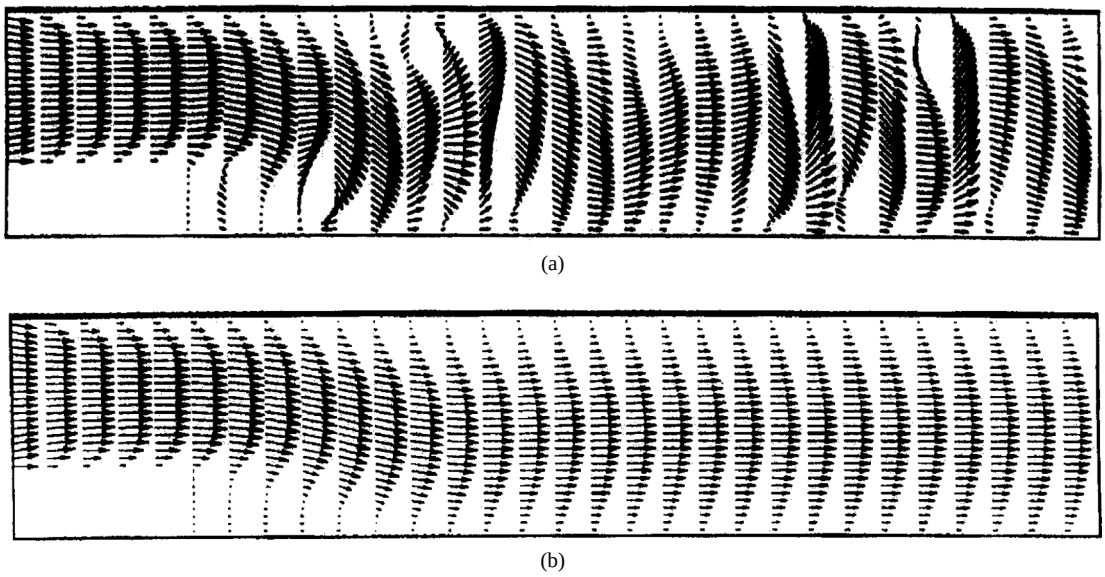

(a)

(b)

Fig. 2. Velocity vector using different scheme: (a) QUICK ($Re = 300$, $Er = 1.5$, 62×32 uniform grid); (b) SGSD ($Re = 300$, $Er = 1.5$, 62×32 uniform grid).

Lee [3]; (3) Feedback sensitivity analysis method proposed by Leonard [4] and the sign preservation principle [1]. All these analysis methods are based on the following five assumptions:

(1) one dimensional equation;
(2) linear problem, both velocity and diffusivity are known and constant;
(3) first kind boundary condition at the two boundaries, i.e., two-point boundary value problem;
(4) uniform grid system;
(5) no variable source term.

Numerical practices show that any deviation from the above assumptions will enhance the stability. And the critical Peclet number resulted from the existing analysis methods gives us the most severe condition. For example, the critical Peclet number of the central difference scheme is usually known as 2. However, we may get a non-oscillating solution even if the local Peclet number is as large as 180 for some practical problems [5,6]. Thus how to obtain the critical Peclet number of those conditionally stable schemes when applied to complicated multi-dimensional problems remain unresolved.

1.3. An absolutely stable and at least second-order accuracy scheme—SGSD

It is a common understanding in the computational heat transfer community that the stability and accuracy of the discretized convective term constitute a contradicting pair [7]. For example, the first upwind scheme is absolutely stable with severe false diffusion, while the 2nd order or 3rd order accurate schemes such as CD, QUICK and TUD are only conditionally stable. This situation has been somewhat changed since the introduction of SGSD scheme in [8].

A new scheme called SGSD (stability guaranteed second-order difference scheme) was proposed in [8] which is absolutely stable and possesses at least second-order accuracy. The scheme is based on another scheme called SCSD (stability controllable second-order difference scheme) proposed in [9]. In the SCSD scheme the general variables at the interfaces e and w are defined as follows:

$$\begin{aligned} \phi_e &= \beta\phi_e^{\mathrm{CD}} + (1-\beta)\phi_e^{\mathrm{SUD}} \\ \phi_w &= \beta\phi_w^{\mathrm{CD}} + (1-\beta)\phi_w^{\mathrm{SUD}} \end{aligned} \tag{3}$$

where the superscripts CD and SUD refer to the central difference and second-order upwind difference scheme. By changing the value of β (between 0 and 1), the critical Peclet number of the SCSD scheme varies from 2 (when $\beta = 1$) to infinite (when $\beta = 0$). It is obvious that the selection of β is the key issue in applying SCSD. This issue has been successfully resolved in SGSD. In the SGSD scheme, the value of β is automatically determined during the computation by following equation:

$$\beta = \frac{2}{2 + |P_\Delta|} \tag{4}$$

where the grid Peclet number P_Δ is defined as

$$P_{\Delta x} = \frac{u\delta x}{\Gamma}, \qquad P_{\Delta y} = \frac{u\delta y}{\Gamma} \tag{5}$$

The accuracy of the SGSD is obviously at least of 2nd order, and it is easy to show that when $\beta = 3/4$, it possesses 3rd order accuracy. Numerical computations for the lid-driven cavity flow with different schemes are compared with the benchmark solutions provided in [10], and the error analyses are presented in Tables 1 and 2. As far as the computational time is concerned, for a uniform grid system, SGSD may

Table 1
Relative error of centerline u-veloctty obtained using uniform grid (42×42), %

y	SGSD	SLID	QUICK	CD
0.9766	0.5961	3.4477	−0.7099	−1.8278
0.9688	0.4940	5.5434	−1.3758	−3.3100
0.9609	−1.6179	5.8356	−4.1650	−7.0329
0.9531	1.7917	10.35210	−1.5664	−5.2377
0.8516	1.6725	14.6770	−4.4679	−10.0559
0.7344	1.0150	13.4836	−4.3165	−9.5678
0.6172	−7.2431	2.9113	−9.8562	−14.5212
0.5000	16.1020	33.9967	5.4276	−1.6118
0.4531	11.0819	27.5451	2.0098	−4.5642
0.2813	8.0669	23.6360	−0.2050	−5.9558
0.1719	−3.1419	6.3830	−7.6654	−12.6041
0.1016	−16.8012	−16.2563	−14.0868	−15.0858
0.0703	−23.0018	−27.9703	−16.1296	−14.2394
0.0625	−24.6782	−31.4765	−16.4884	−13.6463
0.0547	−25.9926	−33.9499	−17.0744	−13.7059
Mean error	9.5531	17.1956	7.0363	8.8644

Table 2
Relative error of centerline v-velocity obtained using uniform grid (42×42), %

x	SGSD	SLID	QUICK	CD
0.9688	−16.4017	−18.2859	−13.1989	−8.1213
0.9609	−14.9011	−17.2648	−11.9592	−7.0584
0.9531	−14.2403	−15.8331	−11.7725	−8.6462
0.9453	−12.5216	−11.5934	−10.3577	−8.4337
0.9063	−4.9311	0.57807	−7.0805	−10.5936
0.8594	3.1407	16.0975	−2.6930	−7.7979
0.8047	2.5182	14.1713	−2.8592	−7.6018
0.5000	−12.6286	−20.8630	−4.7901	4.1171
0.2344	0.5708	10.8422	−4.0980	−8.2425
0.2266	0.1746	10.6848	−4.4293	−8.6984
0.1563	−1.7118	9.0362	−6.7151	−11.8210
0.0938	−3.3040	6.5743	−7.6163	−12.7747
0.0781	−3.8282	5.7028	−7.9530	−13.0695
0.0703	−3.9121	5.4735	−7.9691	−13.0842
0.0625	−3.3509	5.9341	−7.3640	−12.5122
Mean error	6.5519	11.3957	7.3904	9.5048

Table 3
Comparison of computational time for lid-driven cavity flow

	SGSD	SUD	QUICK	CD
Uniform grid	1	1.1121	0.7023	0.6018
Nonuniform grid	0.5025	0.5309	0.7139	0.7436

take 20–30% more time than CD or QUICK, while for a nonuniform grid system, SGSD takes less computational time than CD and QUICK. Table 3 gives the comparison for the lid-driven cavity flow computations.

It can be easily shown by the sign preservation principle that with such defined β the scheme is unconditionally stable. Numerical computations for flow over a backward step show that when a solution with QUICK scheme is oscillating (Fig. 2(a), Fig. 3), the solution with SGSD is still physically reasonable (Fig. 2(b), Fig. 3).

The above comparison study shows that SGSD is an attractive scheme for computational heat transfer.

2. Advances in the study of boundedness of discretized convective term

2.1. Is Gaskell/Lau's CBC sufficient and necessary?

Boundedness is an important numerical characteristic of a discretized scheme for the convection term when the problem being solved contains an abrupt change of field variables. In 1988 Gaskell and Lau proposed conditions for scheme to possess the boundedness, and it is called the convective boundedness criterion (CBC) [11].

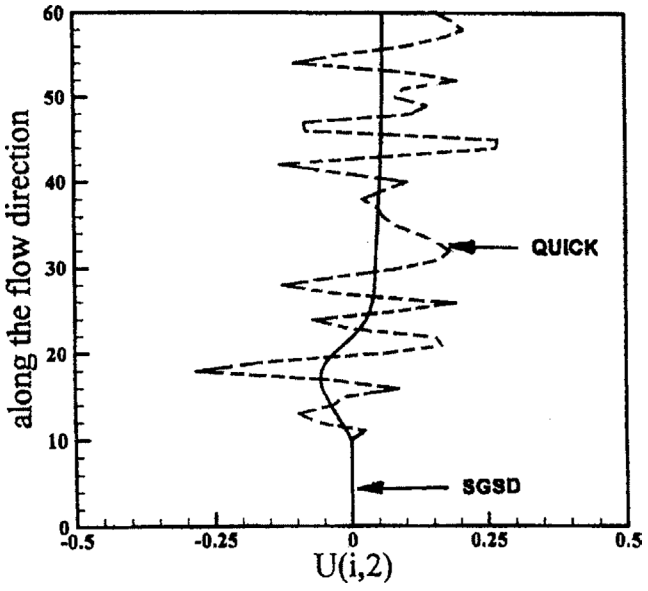

Fig. 3. The u-velocity component at the first control volume surface near the bottom wall ($Re = 300$, 62×32 uniform grid).

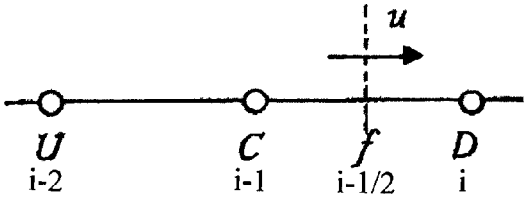

Fig. 4. Interface and its related grid point.

In the finite volume approach, the scheme definition is the interpolation rule for the interface value, and for most schemes used in CFD/NHT it can be expressed as (Fig. 4)

$$\phi = f(\phi_U, \phi_C, \phi_D) \tag{6a}$$

In terms of the normalized general variable defined by

$$\tilde{\phi} = \frac{\phi - \phi_U}{\phi_U - \phi_D} \tag{7}$$

where the subscripts U, D refer to the upstream and downstream points (Fig. 5), Eq. (6a) is simplified as

$$\tilde{\phi} = f(\tilde{\phi}_C) \tag{6b}$$

Gaskell and Lau proposed that a continuous increasing function or a piecewise continuous increasing function $\tilde{\phi} = f(\tilde{\phi}_C)$ will possess the boundedness if following conditions are satisfied:

$$(1)\ \tilde{\phi}_f = f(\tilde{\phi}_C) = \tilde{\phi}_C, \quad \text{for } \tilde{\phi}_C \leqslant 0 \tag{8a}$$

$$(2)\ \tilde{\phi}_f = f(\tilde{\phi}_C) = \tilde{\phi}_C, \quad \text{for } \tilde{\phi}_C \geqslant 1 \tag{8b}$$

$$(3)\ \tilde{\phi}_C \leqslant f(\tilde{\phi}_C) \leqslant 1, \quad \text{for } 0 \leqslant \tilde{\phi}_C \leqslant 1 \tag{8c}$$

The CBC region can be expressed by the shaded area in Fig. 5, where $\tilde{\phi}_f$ and $\tilde{\phi}_C$ serve as the ordinate and the abscissa. If the defining expression of a scheme is located in the shaded area, the scheme possesses the boundedness. This

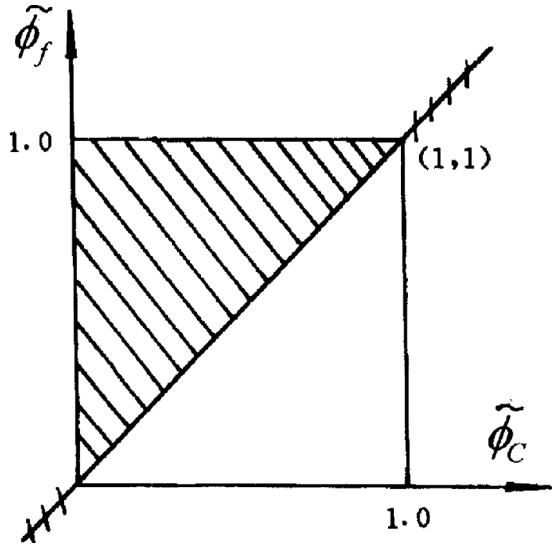

Fig. 5. The CBC region defined by Gaskell/Lau.

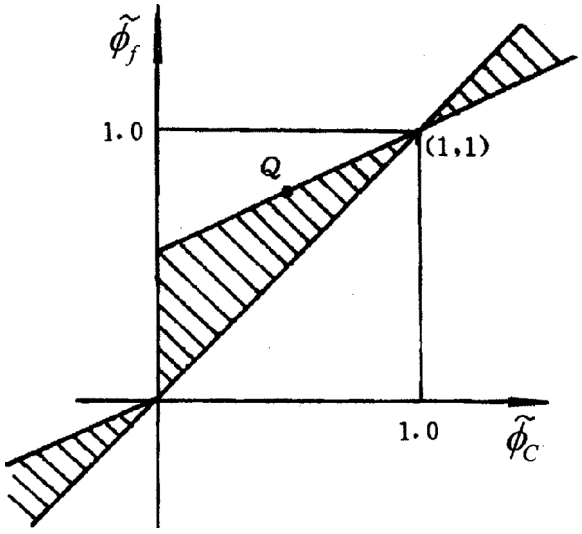

Fig. 6. The CBC region defined by Yu et al.

CBC is usually considered as both necessary and sufficient [11–13]. However, our study shows that this CBC is only sufficient, but is not necessary. To be specific, the first and second conditions are only sufficient, while the third one is both necessary and sufficient. Another region was outlined in [5] (Fig. 6), and two more schemes were proposed whose definitions were located in the new region rather than in the CBC region proposed by Gaskell/Lau. In Refs. [14,15] further discussion was conducted to refine the CBC from different points of view. In the following the results of [15] are briefly presented.

2.2. Refinement of the CBC from the smoothness of interpolation profile

Apart from the necessary and sufficient issue another weakness of the G-L CBC is that not all the schemes which

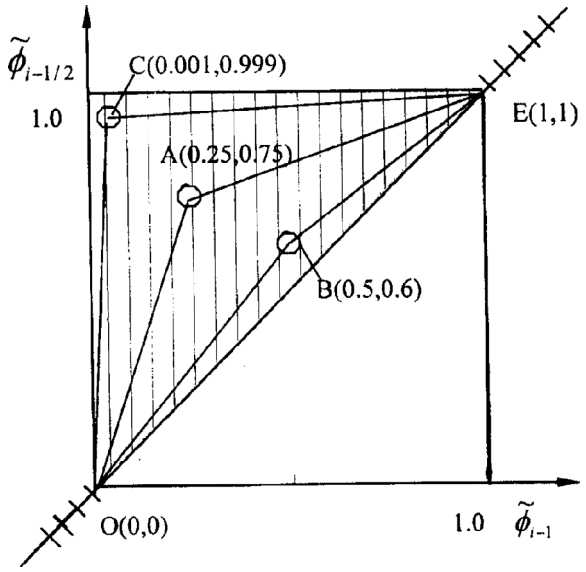

Fig. 7. Three points A, B, and C in G/L CBC region.

satisfy the CBC criterion can get physically reasonable solution. For example, if we take three points A, B, C in the Gaskell/Lau CBC region shown in Fig. 7, then the resulting profiles of the field variable variation are presented in Fig. 8. Obviously such variation patterns are quite odd and unrealistic.

By careful consideration of the smoothness of the profile pattern of the normalized variable, a new CBC is proposed in [15], which says: For a continuous or piecewise continuous function $\tilde{\phi} = f(\tilde{\phi}_C)$, if following conditions are satisfied, the scheme represented by $f(\tilde{\phi}_C)$ possesses both boundedness and high accuracy:

$$
\begin{aligned}
&\text{(1) for } \tilde{\phi}_C \in (1, +\infty),\ f(\tilde{\phi}_C) \in \left(0.5(1+\tilde{\phi}_C), \tilde{\phi}_C\right]\\
&\text{(2) for } \tilde{\phi}_C \in (-\infty, 0),\ f(\tilde{\phi}_C) \in [\tilde{\phi}_C, 0.5\tilde{\phi}_C)\\
&\text{(3) for } \tilde{\phi}_C \in [0, 0.5),\ f(\tilde{\phi}_C) \in \left(1.5\tilde{\phi}_C, 0.5(1+\tilde{\phi}_C)\right]\\
&\text{(4) for } \tilde{\phi}_C \in (1/2, 2/3),\ f(\tilde{\phi}_C) \in \left[0.5(1+\tilde{\phi}_C), 1.5\tilde{\phi}_C\right)\\
&\text{(5) for } \tilde{\phi}_C \in [2/3, 1],\ f(\tilde{\phi}_C) \in \left(0.5(1+\tilde{\phi}_C), 1\right] \qquad (9)
\end{aligned}
$$

This criterion is presented in Fig. 9 by the shaded area. In [14] different considerations are given to the interpolation value: the interfacial variable should have a positive response to the disturbance of variable at grid points and the transportive property should be kept. The resulted CBC region $\tilde{\phi}_C \in [1, 1.0]$ coincides with the one presented in Fig. 9. Up to date at least eleven higher-order composite schemes were proposed which possess the boundedness character. It is easy to show that all the existing higher-order bounded schemes are located in this new region (Table 4).

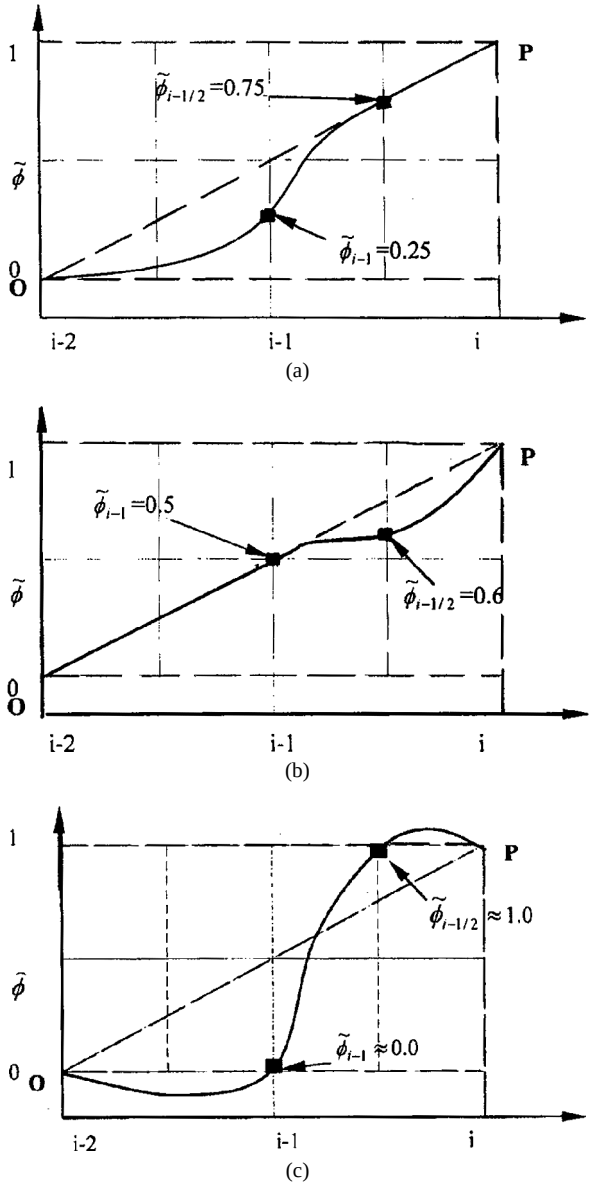

Fig. 8. Three unrealistic situations: (a) Point A; (b) Point B; (c) Point C.

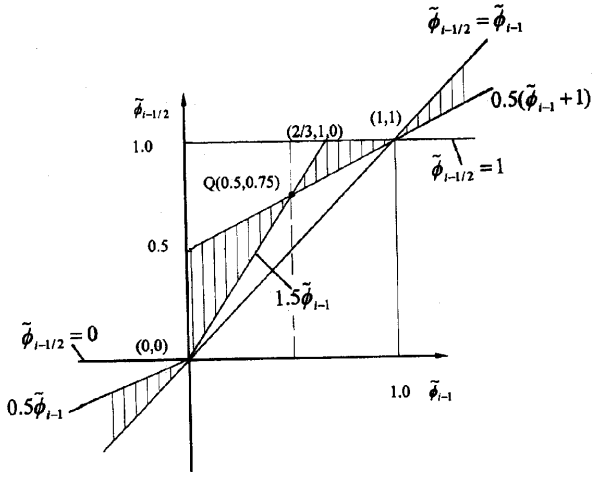

Fig. 9. CBC region of Hou et al.

Table 4
Existing bounded composite schemes

No.	Scheme	Definition with normalized variable	Normalized variable diagram
1 [12]	COPLA (combination of piecewise linear approximation)	$\tilde{\phi}_{i-1/2} = \begin{cases} 2.25\tilde{\phi}_{i-1} & 0 \leqslant \tilde{\phi}_{i-1} \leqslant 1/4 \\ \frac{3}{8} + \frac{3}{4}\tilde{\phi}_{i-1} & \frac{1}{4} \leqslant \tilde{\phi}_{i-1} \leqslant \frac{3}{4} \\ \frac{3}{4} + \frac{1}{4}\tilde{\phi}_{i-1} & \frac{3}{4} \leqslant \tilde{\phi}_{i-1} \leqslant 1 \\ \tilde{\phi}_{i-1} & \text{else} \end{cases}$	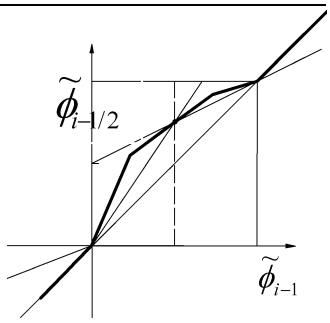
2 [16]	EULER	$\tilde{\phi}_{i-1/2} = \begin{cases} \frac{\sqrt{\tilde{\phi}_{i-1}(1-\tilde{\phi}_{i-1})^3} - \tilde{\phi}_{i-1}^2}{1-2\tilde{\phi}_{i-1}} & 0 \leqslant \tilde{\phi}_{i-1} \leqslant 1 \\ 3/4 & \tilde{\phi}_{i-1} = 0.5 \\ \tilde{\phi}_{i-1} & \text{else} \end{cases}$	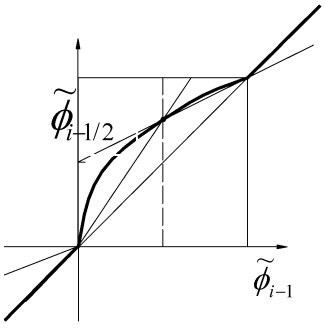
3 [17]	CLAM (hybrid linear/parabolic approximation)	$\tilde{\phi}_{i-1/2} = \begin{cases} \tilde{\phi}_{i-1}(2 - \tilde{\phi}_{i-1}) & 0 \leqslant \tilde{\phi}_{i-1} \leqslant 1 \\ \tilde{\phi}_{i-1} & \text{else} \end{cases}$	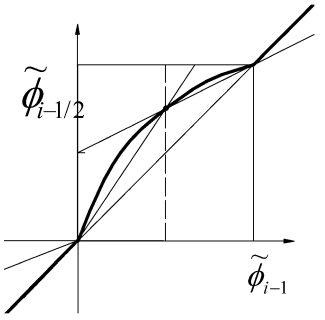
4 [13]	MINMOD (minimum modulus)	$\tilde{\phi}_{i-1/2} = \begin{cases} \frac{3}{2}\tilde{\phi}_{i-1} & 0 \leqslant \tilde{\phi}_{i-1} \leqslant \frac{1}{2} \\ \frac{1}{2}(1 + \tilde{\phi}_{i-1}) & 0.5 \leqslant \tilde{\phi}_{i-1} \leqslant 1 \\ \tilde{\phi}_{i-1} & \text{else} \end{cases}$	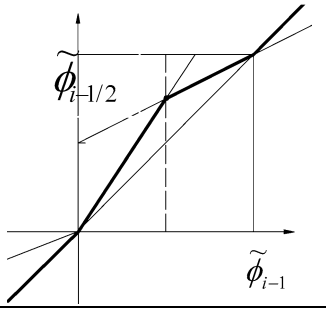

3. Advances in the study of coupling between velocity and pressure

The pressure-correction method is probably the most widely adopted method for solving incompressible flow problem. The first pressure-correction algorithm was SIMPLE proposed by Patankar and Spalding in 1972 [22]. The acronym SIMPLE stands for semi-implicit method for the pressure-linked equation. The major approximations made in the SIMPLE algorithm are: (1) The initial pressure field and the initial velocity fields are independently assumed, hence the inherent interconnection between pressure and velocities is neglected, leading to some inconsistency between them; (2) The effects of the pressure corrections of the neighboring grids are arbitrarily dropped in order to simplify the solution procedure, thus make the algorithm semi-implicit.

Table 4 (*Continued*)

No.	Scheme	Definition with normalized variable	Normalized variable diagram
5 [18]	MUSCL (monotonic upwind scheme for conservation law)	$\tilde{\phi}_{i-1/2} = \begin{cases} 2\tilde{\phi}_{i-1} & 0 \leqslant \tilde{\phi}_{i-1} \leqslant 1/4 \\ 1/4 + \tilde{\phi}_{i-1} & \frac{1}{4} \leqslant \tilde{\phi}_{i-1} \leqslant \frac{3}{4} \\ 1 & \frac{3}{4} \leqslant \tilde{\phi}_{i-1} \leqslant 1 \\ \tilde{\phi}_{i-1} & \text{else} \end{cases}$	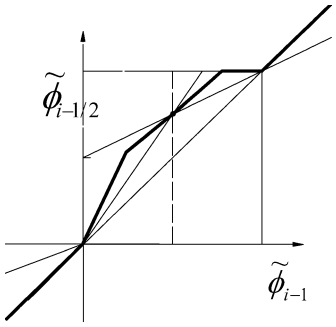
6 [19]	OSHER	$\tilde{\phi}_{i-1/2} = \begin{cases} \frac{3}{2}\tilde{\phi}_{i-1} & 0 \leqslant \tilde{\phi}_{i-1} \leqslant 2/3 \\ 1 & 2/3 \leqslant \tilde{\phi}_{i-1} \leqslant 1 \\ \tilde{\phi}_{i-1} & \text{else} \end{cases}$	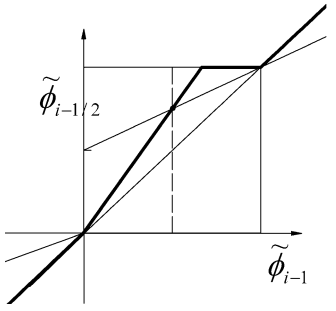
7 [5]	SECBC (scheme based on extended CBC)	$\tilde{\phi}_{i-1/2} = \begin{cases} \frac{1}{2}\tilde{\phi}_{i-1} & \tilde{\phi}_{i-1} \leqslant 0 \\ 3\tilde{\phi}_{i-1} & 0 < \tilde{\phi}_{i-1} < 0.2 \\ \frac{\tilde{\phi}_{i-1}+1}{2} & \tilde{\phi}_{i-1} \geqslant 0.2 \end{cases}$	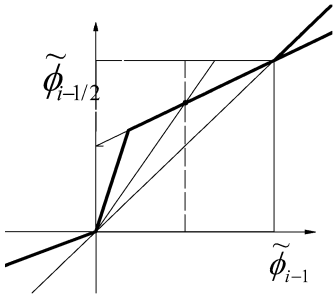
8 [11]	SMART (sharp and monotonic algorithm for realistic transport)	$\tilde{\phi}_{i-1/2} = \begin{cases} 3\tilde{\phi}_{i-1} & 0 \leqslant \tilde{\phi}_{i-1} \leqslant 1/6 \\ 3/8 + 3/4\tilde{\phi}_{i-1} & \frac{1}{6} \leqslant \tilde{\phi}_{i-1} \leqslant \frac{5}{6} \\ 1 & \frac{5}{6} \leqslant \tilde{\phi}_{i-1} \leqslant 1 \\ \tilde{\phi}_{i-1} & \text{else} \end{cases}$	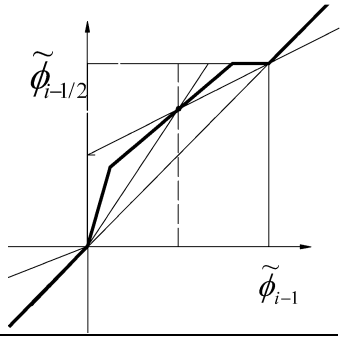

These assumptions will not affect the final solutions if the iterative process converges [2]. However, they do affect the convergence rate. Therefore, since the proposal of the SIMPLE algorithm, a number of its variants were proposed in order to overcome one or both of the approximations [23–35].

The SIMPLER algorithm [23] successfully overcomes the first approximation, and is widely used in the current CFD/NHT community. Even though there are more than ten variants of the SIMPLE-like algorithm, the second approximation, i.e., the dropping of the neighboring grid effects, have not been successfully resolved so far. These variants include SIMPLEC and SIMPLEX by van Doormaal and Raithby in 1984 and 1985 [24–26], PISO by Issa in 1985 [27] and the revised versions by Connell and Stow in 1986 [28], Chatwani and Turan in 1991 [29], Lee and Tzong in 1992 [30], Yen and Liu in 1993 [31], Wen and Ingham [32] in 1993, SIMPLESSEC, SIMPLESSE by Gjesdal and Lossius [33] in 1997, SIMPLET by Sheng et al. in 1998 [34],

Table 4 (*Continued*)

No.	Scheme	Definition with normalized variable	Normalized variable diagram
9 [20]	STOIC (second and third order interpolation for convection)	$\tilde{\phi}_{i-1/2} = \begin{cases} 3\tilde{\phi}_{i-1} & 0 \leqslant \tilde{\phi}_{i-1} \leqslant 1/5 \\ 1/2(1+\tilde{\phi}_{i-1}) & \frac{1}{5} \leqslant \tilde{\phi}_{i-1} \leqslant 1/2 \\ \frac{3}{8} + \frac{3}{4}\tilde{\phi}_{i-1} & \frac{1}{2} \leqslant \tilde{\phi}_{i-1} \leqslant \frac{5}{6} \\ 1 & \frac{5}{6} \leqslant \tilde{\phi}_{i-1} \leqslant 1 \\ \tilde{\phi}_{i-1} & \text{else} \end{cases}$	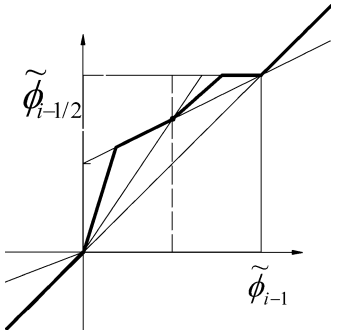
10 [21]	WACEB (weighted-average coefficient ensuring boundedness)	$\tilde{\phi}_{i-1/2} = \begin{cases} 2\tilde{\phi}_{i-1} & 0 \leqslant \tilde{\phi}_{i-1} \leqslant 0.3 \\ 3/8 + 3/4\tilde{\phi}_{i-1} & 0.3 \leqslant \tilde{\phi}_{i-1} \leqslant \frac{5}{6} \\ 1 & \frac{5}{6} \leqslant \tilde{\phi}_{i-1} \leqslant 1 \\ \tilde{\phi}_{i-1} & \text{else} \end{cases}$	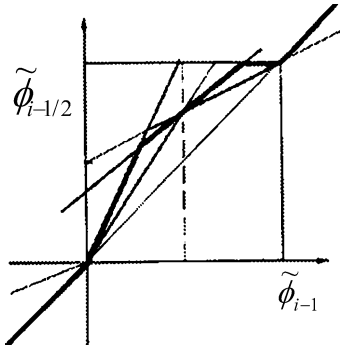
11 [14]	HOAB (high-order-accurate bounded scheme)	$\tilde{\phi}_{i-1/2} = \begin{cases} 3.5\tilde{\phi}_{i-1} & 0 < \tilde{\phi}_i \leqslant 1/6 \\ 0.5\tilde{\phi}_i + 0.5 & 1/6 < \tilde{\phi}_i \leqslant 0.5 \\ \tilde{\phi}_i + 0.25 & 0.5 < \tilde{\phi}_i \leqslant 0.75 \\ 1_i & 0.75 < \tilde{\phi}_i \leqslant 1 \\ \tilde{\phi}_i & \text{elsewhere} \end{cases}$	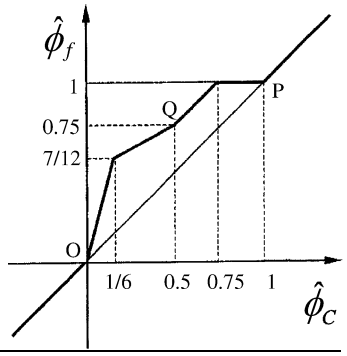

MSIMPLER by Yu et al. in 2001 [35]. All these variants are usually called SIMPLE-like or SIMPLE-family algorithm. The character common to all these algorithms is that a pressure correction term is introduced to the segregated solution process to improve the velocity, and the effects of the pressure corrections of the neighboring grid points are neglected. Because of this basic feature, the improvement in the convergence rate of the above proposed variants are limited, usually in the order of tens of percent. Recently, Moukalled and Darwish [36] made a comprehensive review and reorganization of the express format for all the pressure correction algorithms.

The function of the pressure correction term in the SIMPLE-family algorithms is to improve the current pressure and velocity by adding their corresponding corrections such that the resulting improved velocity can satisfy the mass conservation condition at each iteration level. And this is of crucial importance to accelerate the iteration convergence, as has been clearly demonstrated in [37]. In [38,39] a new idea of improving velocity and pressure is proposed: the improved velocity and pressure of each iteration level are not determined by adding a correction term to their temporary solution; instead, they are directly solved from the momentum and continuity equations, genuinely avoiding the introduction of pressure correction term and velocity correction term. Thus the second approximation of the SIMPLE algorithm is totally discarded, making the algorithm fully implicit. The novel algorithm is named CLEAR, standing for **C**oupled & **L**inked **E**quations **A**lgorithm **R**evised. Because of this key improvement, the convergence rate of the iterative procedure can be drastically increased, and the enhancement ratio ranges from several times to tens of percent.

3.1. Brief introduction to CLEAR algorithm

Taking 2-D problem as an example, the resulting formulation of the discretization equation takes following form:

$$a_P\phi_P = a_E\phi_E + a_W\phi_W + a_N\phi_N + a_S\phi_S + b \tag{10}$$

Underrelaxation of the dependent variables is incorporated into the solution process of the algebraic equations, then Eq. (10) becomes:

$$\frac{a_p}{\alpha}\phi_P = a_E\phi_E + a_W\phi_W + a_N\phi_N + a_S\phi_S + b + \frac{1-\alpha}{\alpha}a_p\phi_P^0 \tag{11}$$

The denominator of the left-hand side term and the last term at the right hand side of Eq. (11) are the outcome of this underrelaxation process. For velocity components, the pressure gradient term is usually separated from the source term b. With a pressure field solved from the velocity of the previous iteration, the temporary or intermediate velocity solution of the current iteration, u^*, v^*, can be expressed by Eqs. (12a) and (12b).

$$\frac{a_e}{\alpha_u}u_e^* = \sum a_{nb}u_{nb}^* + b + A_e(p_P^* - p_E^*) + A_e\frac{1-\alpha_u}{\alpha_u}a_e u_e^0 \tag{12a}$$

$$\frac{a_n}{\alpha_v}v_n^* = \sum a_{nb}v_{nb}^* + b + A_n(p_P^* - p_N^*) + A_n\frac{1-\alpha_v}{\alpha_v}a_n v_n^0 \tag{12b}$$

where u^0, v^0 denote the solutions of u and v of the previous iteration.

In the following presentation, we first briefly describe the computational process of SIMPLER algorithm, and introduce the main idea of CLEAR at some appropriate point.

The intermediate values of velocity and pressure have to be modified, so that the updated velocity satisfies the discretized continuity equation. In order to get an improved velocity field, velocity correction terms, denoted by u', v', and a corresponding pressure correction term, denoted by p', are introduced. The improved pressure and velocities are expressed as follows:

$$p = p^* + p' \tag{13a}$$

$$u_e = u_e^* + u_e'$$

$$v_n = v_n^* + v_n' \tag{13b}$$

The improved pressure and velocities are then substituted into the discretized momentum equation, Eq. (12a), yielding

$$\frac{a_e}{\alpha_u}(u_e^* + u_e') = \sum a_{nb}(u_{nb}^* + u_{nb}') + b + A_e\big[(p_P^* + p_P') - (p_E^* + p_E')\big] + A_e\frac{1-\alpha_u}{\alpha_u}a_e u_e^0 \tag{14}$$

Subtracting Eq. (12a) from Eq. (14), the equation of velocity correction u_e' is obtained:

$$\frac{a_e}{\alpha_u}u_e' = \sum a_{nb}u_{nb}' + A_e(p_P' - p_E') \tag{15}$$

Similarly for v component, we have:

$$\frac{a_n}{\alpha_v}v_n' = \sum a_{nb}v_{nb}' + A_n(p_P' - p_N') \tag{16}$$

From Eqs. (15) and (16), it can be found that the velocity correction term includes two parts: the velocity correction in the vicinity of the control volume and the difference of pressure correction of two adjacent grid points. In SIMPLE-like methods, the term $\sum a_{nb}u_{nb}'$ is neglected in order to make the final pressure correction equation manageable [2]. The final velocity correction are expressed in the following forms:

$$u_e' = d_e(p_P' - p_E') \tag{17a}$$

$$v_n' = d_n(p_P' - p_N') \tag{17b}$$

where

$$d_e = \frac{A_e\alpha_u}{a_e} \tag{18a}$$

$$d_n = \frac{A_n\alpha_v}{a_n} \tag{18b}$$

The improved velocities, $u = u^* + u'$, $v = v^* + v'$, are substituted into the discretized continuity Eq. (19)

$$(\rho u)_e A_e - (\rho u)_w A_w + (\rho v)_n A_n - (\rho v)_s A_s = 0 \tag{19}$$

the final pressure correction equation is obtained as follows:

$$a_P p_P' = \sum a_{nb}p_{nb}' + b \tag{20}$$

where

$$a_P = a_E + a_W + a_N + a_S \tag{21a}$$

$$a_E = (\rho Ad)_e, \qquad a_W = (\rho Ad)_w$$

$$a_N = (\rho Ad)_n, \qquad a_S = (\rho Ad)_s \tag{22b}$$

$$b = (\rho u^* A)_w - (\rho u^* A)_e + (\rho v^* A)_s - (\rho v^* A)_n \tag{22c}$$

In the SIMPLER algorithm, the pressure correction is only used to modify velocity. The pressure is determined by pressure equation, which is derived as follows. The u-momentum equation can be re-cast into

$$u_e = \frac{\sum a_{nb}u_{nb} + b}{a_e} + d_e(p_P - p_E) = \tilde{u}_e + d_e(p_P - p_E) \tag{23}$$

where $\tilde{u}_e$ is called pseudo-velocity. Similarly, for v component we have

$$v_n = \tilde{v}_n + d_n(p_P - p_N) \tag{24}$$

Again substituting Eqs. (23), (24) into continuity Eq. (19), we obtain the pressure equation as follows:

$$a_P p_P^* = \sum a_{nb}p_{nb}^* + b \tag{25}$$

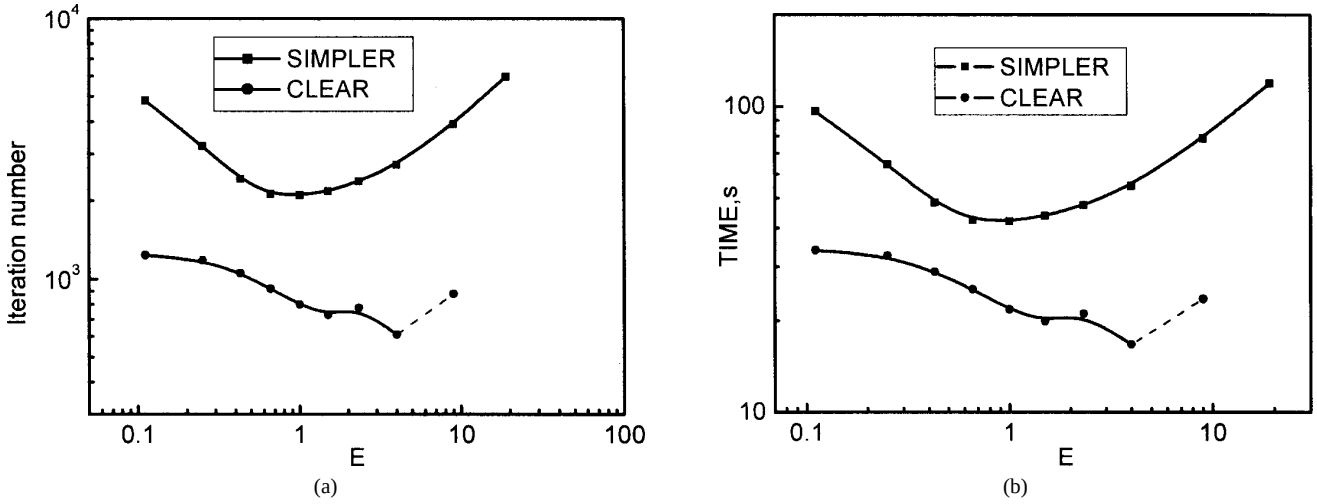

Fig. 10. Comparison of iteration numbers and CPU time for $Re = 1000$ of Example 1 (lid-driven square cavity flow). (a) Iteration number; (b) CPU time.

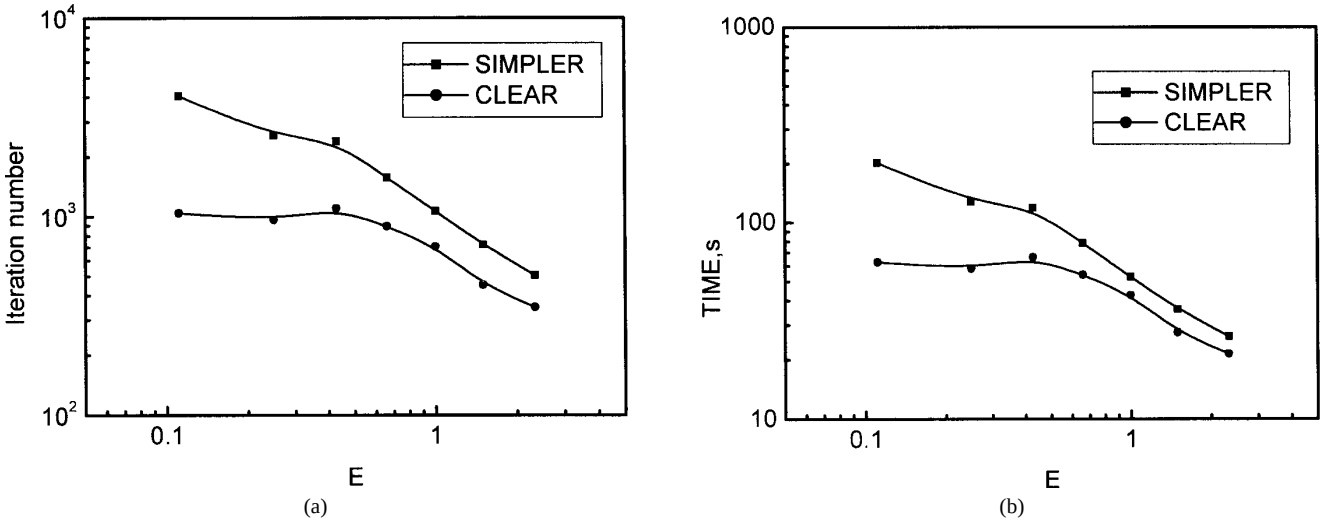

Fig. 11. Comparison of iteration number and CPU time for $Re = 200$ of Example 2 (heat transfer in a sudden enlarge tube). (a) Iteration number; (b) CPU time.

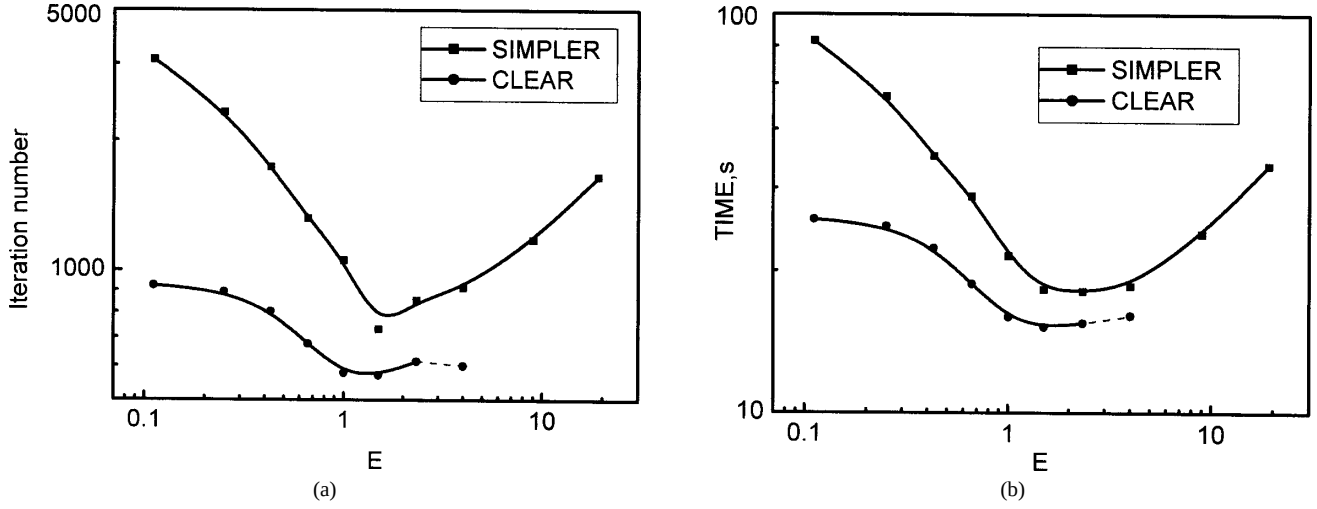

Fig. 12. Comparison of iteration number and CPU time for $Re = 1000$ of Example 3 (lid-driven annular cavity flow). (a) Iteration number; (b) CPU time.

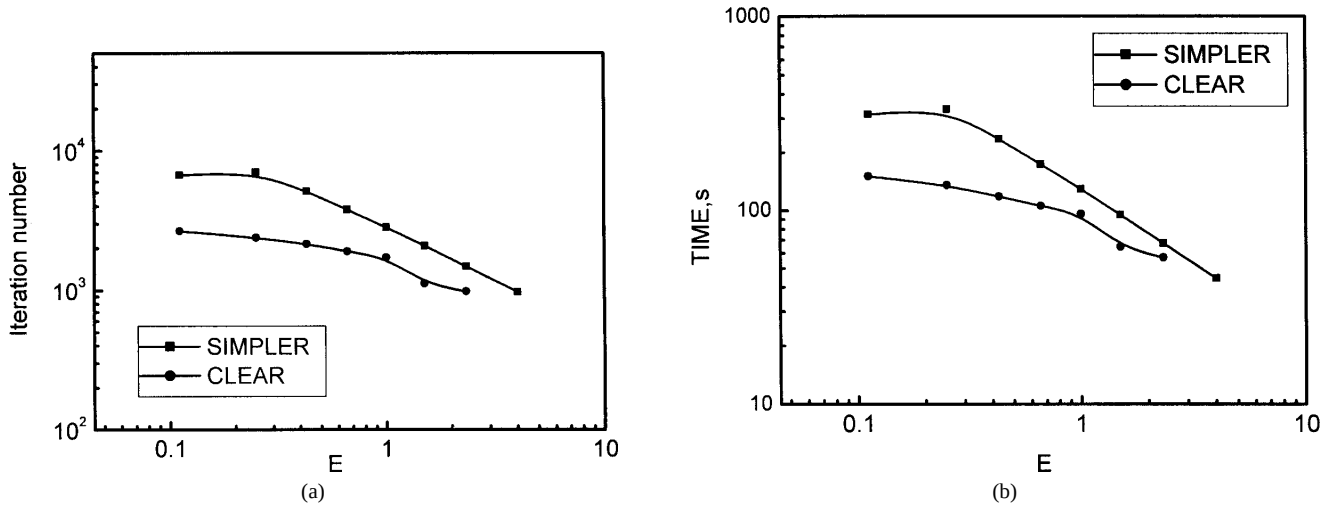

Fig. 13. Comparison of iteration number and CPU time for $Re = 300$ of Example 4 (flow over a rectangular back step). (a) Iteration number; (b) CPU time.

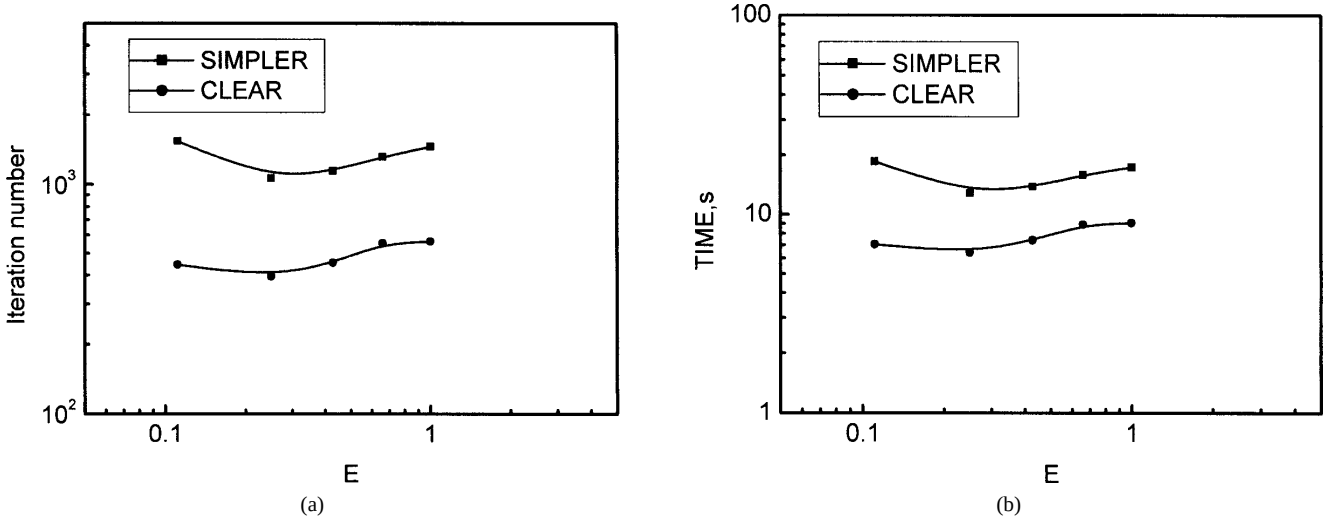

Fig. 14. Ratios of iteration numbers and CPU time of Example 5 (natural convection in an annulus). (a) Iteration number; (b) CPU time.

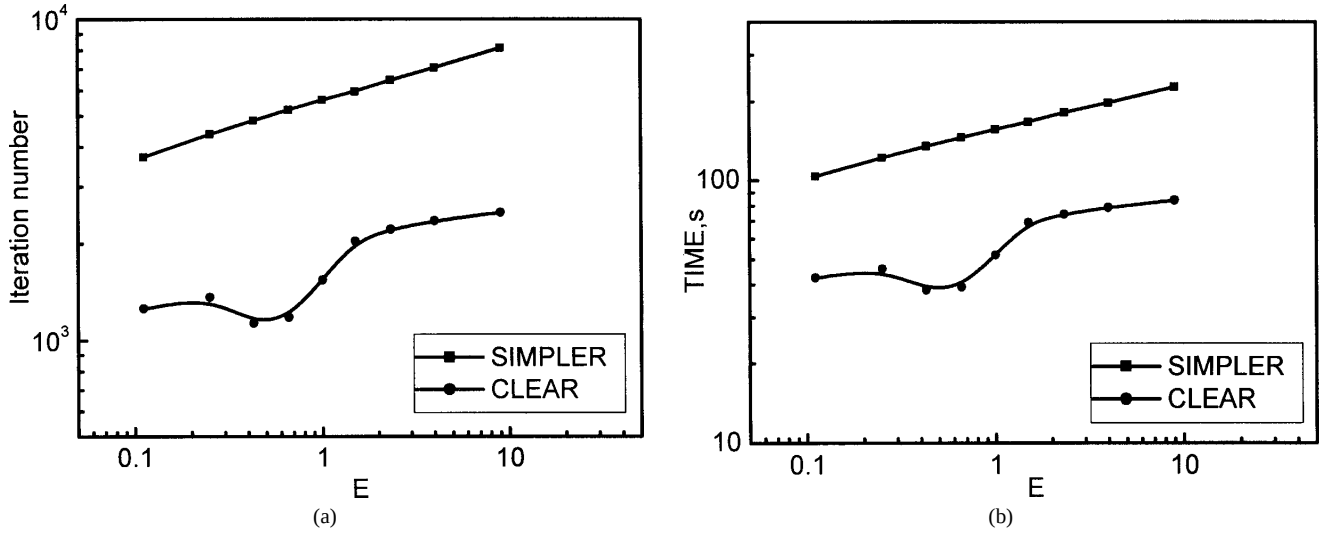

Fig. 15. Comparison of iteration number and CPU time for $Ra = 10^6$ of Example 6 (natural convection in a square cavity). (a) Iteration number; (b) CPU time.

where

$$a_P = a_E + a_W + a_N + a_S \tag{26a}$$

$$a_E = (\rho A d)_e, \qquad a_W = (\rho A d)_w$$

$$a_N = (\rho A d)_n, \qquad a_S = (\rho A d)_s \tag{26b}$$

$$b = \left(\rho \tilde{u}^0 A\right)_w - \left(\rho \tilde{u}^0 A\right)_e + \left(\rho \tilde{v}^0 A\right)_s - \left(\rho \tilde{v}^0 A\right)_n \tag{26c}$$

From the above derivation, we can see that the intermediate value u^*, v^* satisfy momentum equation, and the improved value u_e, v_n satisfy the continuity equation. The improved values are taken as the solution of the current iteration level to start the next iteration. Then the consistency condition is satisfied for the singular coefficient matrix of velocity, and the convergence rate can be accelerated [37]. The converged solution we are searching for is the one which satisfies both the momentum equation and the continuity equation.

We now propose a new expression for improved velocity. In the correction stage, the temporary solution of the current iteration in the SIMPLER algorithm is expressed as

$$u_e = u_e^* + d_e(p'_P - p'_E) \tag{27}$$

Eq. (27) is similar to Eq. (23) where the pseudo-velocity is introduced. And for the convenience of discussion Eq. (23) is re-written as follows:

$$u_e = \tilde{u}_e + d_e(p_P - p_E) \tag{28}$$

Here $\tilde{u}_e$ and u_e^* are at the same position, and term $(p_P - p_E)$ and $(p'_P - p'_E)$ play a similar role in the two equations. Hence we may assume that in the corrector step, the improved velocity, u and v, and the improved pressure, p, can be related by the same format of equation:

$$u_e = \tilde{u}_e^* + d_e(p_P - p_E) \tag{29a}$$

$$v_n = \tilde{v}_n^* + d_n(p_P - p_N) \tag{29b}$$

where the pseudo-velocity, $\tilde{u}^*$, $\tilde{v}^*$, are based on the temporary solution u^*, v^*, and can be determined after the momentum equations have been solved. Eqs. (29a) and (29b) are the expressions for the improved velocity in the new algorithm. As will be seen later, it is these new expressions that avoid neglecting some terms in deriving the equation for the improved pressure.

In order to set an extra access for controlling the convergence process, in the determination of the new (or updated) pseudo-velocity an extra relaxation factor, β, is introduced, and the improved velocity is re-written as

$$u_e = \frac{\sum a_{nb} u_{nb}^* + b + \frac{1-\beta_u}{\beta_u} a_e u_e^*}{a_e/\beta_u} + d_e(p_P - p_E)$$
$$= \tilde{u}_e^* + d_e(p_P - p_E) \tag{30a}$$

$$v_n = \frac{\sum a_{nb} v_{nb}^* + b + \frac{1-\beta_v}{\beta_v} a_n v_n^*}{a_n/\beta_v} + d_n(p_P - p_N)$$
$$= \tilde{v}_n^* + d_n(p_P - p_N) \tag{30b}$$

Hereafter β is called the second relaxation factor.

The improved velocity should satisfy the mass conservation condition. Thus substituting Eqs. (30a), (30b) into Eq. (19), we get the equation for the improved pressure:

$$a_P p_P = \sum a_{nb} p_{nb} + b \tag{31}$$

where

$$a_P = a_E + a_W + a_N + a_S \tag{32a}$$

$$a_E = (\rho A d)_e, \qquad a_W = (\rho A d)_w$$

$$a_N = (\rho A d)_n, \qquad a_S = (\rho A d)_s \tag{32b}$$

$$b = (\rho \tilde{u}^* A)_w - (\rho \tilde{u}^* A)_e + (\rho \tilde{v}^* A)_s - (\rho \tilde{v}^* A)_n \tag{32c}$$

the coefficients a_E, a_W, a_N, a_S are calculated based on the intermediate field u^*, v^* with the same expressions shown in Eq. (26b).

Once the improved pressure is solved, the improved velocities can be determined by Eqs. (29a), (29b), which satisfy the continuity condition. In the above derivation, we do not neglect any term, making the solution algorithm fully implicit. Compared with the SIMPLE-like algorithms, it can be stated that the effects of the neighboring grid points are totally taken into account by introducing the updated pseudo-velocity based on u^* and v^*. The above solution algorithm is called CLEAR.

The solution procedure of the CLEAR algorithm is summarized as follows:

Step 1: Assuming an initial velocity field u^0, v^0;

Step 2: Calculating the coefficient of the discretized momentum equation and pseudo-velocity $\tilde{u}^0$, $\tilde{v}^0$:

$$\tilde{u}_e^0 = \frac{\sum a_{nb} u_{nb}^0 + b}{a_e}$$
$$\tilde{v}_n = \frac{\sum a_{nb} v_{nb}^0 + b}{a_n} \tag{33}$$

Step 3: Solving the pressure equation (25) and obtaining pressure field p^*;

Step 4: Based on p^*, solving the momentum equation (12a), (12b), obtaining the intermediate velocity field u^*, v^*;

Step 5: Recalculating the coefficient of momentum equation and the pseudo-velocity $\tilde{u}^*$, $\tilde{v}^*$ based on the intermediate velocity solution u^*, v^*:

$$\tilde{u}_e^* = \frac{\sum a_{nb} u_{nb}^* + b + \frac{1-\beta_u}{\beta_u} a_e u_e^*}{a_e/\beta_u} \tag{34a}$$

$$\tilde{v}_n^* = \frac{\sum a_{nb} v_{nb}^* + b + \frac{1-\beta_v}{\beta_v} a_n v_n^*}{a_n/\beta_v} \tag{34b}$$

Step 6: Solving Eq. (31) for the improved pressure field;

Step 7: Improving the velocity with Eqs. (29a), (29b) to obtain the solution of the present iteration.

Step 8: Solving the discretization equations of the other scalar variables if necessary;

Step 9: Returning to step 2 and repeat until convergence is reached.

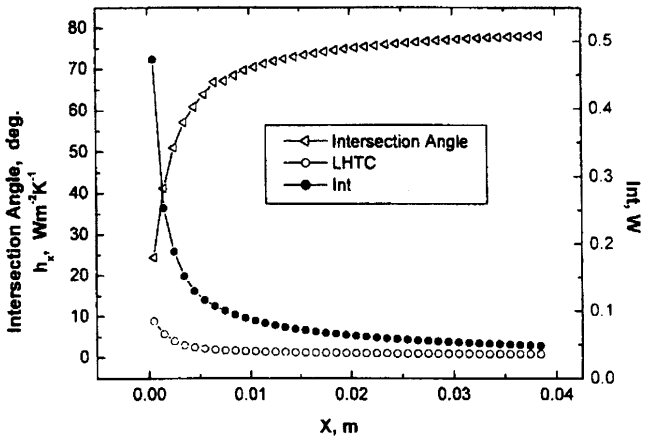

Fig. 16. The distributions of Int, hx and synergy angle along the flow direction.

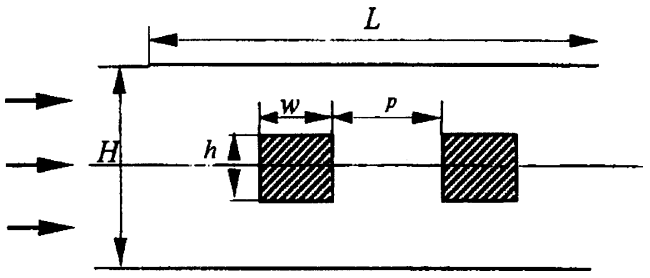

Fig. 17. Parallel plate duct with insertion.

3.2. The second relaxation factor

In determining the updated pseudo-velocity of step 5, we introduce the second relaxation factor β. This is based on the following consideration. As indicated above, the improved velocity and pressure are in full consistency. The good coupling between the pressure and velocity in the CLEAR algorithm can appreciably enhance the convergence rate. This implies that the changes of the velocity solution between two successive iterations are usually larger than those of the SIMPLER algorithm. For the iteration solution procedure of a non-linear problem, experiences show that too large variation of the dependent variables between two successive iterations may lead to diverge of the iteration process [40]. Therefore the second relaxation factor β is introduced in step 5 to present an extra access for controlling the iteration process. From Eqs. (30a), (30b) it can be observed that β appears in both the denominator and nominator. However, the relaxation part is usually not dominated compared to the other terms. Thus a larger value of β will lead to a larger value of the updated value of the pseudo-velocity, hence alleviates the burden of the pressure gradient term, and reduces the variation rate of the two successive iterations. Therefore the second relaxation factor may take values varying in a wide range. If $\beta > 1$, the updated pseudo-velocity is overrelaxed, while the pressure is somewhat underrelaxed; if $\beta < 1$, the situation is the opposite. For simplicity, we set

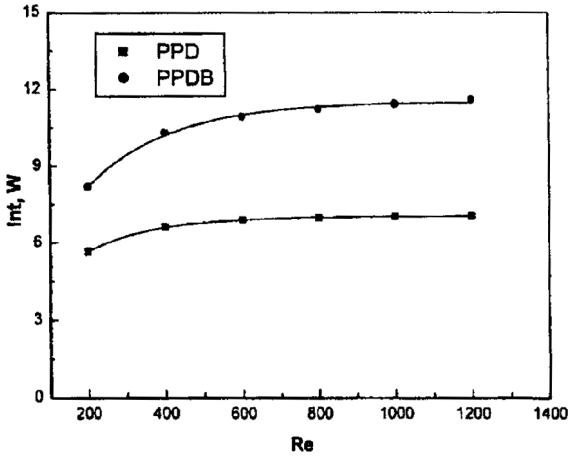

(a)

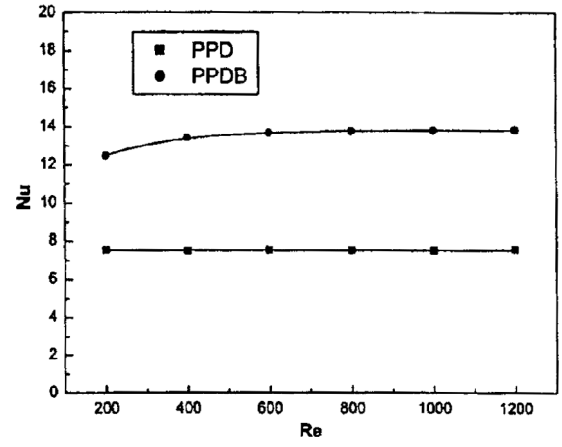

(b)

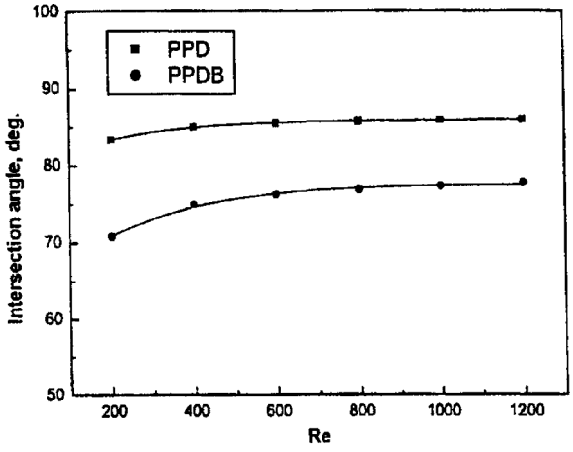

(c)

Fig. 18. Comparisons of the ducts with (PPDB) and without insertions (PPD). (a) Int vs. Re; (b) Nu vs. Re; (c) θ_m vs. Re.

the following relation between the two relaxation factors β and α in the computations of the six examples presented below:

$$\beta = \begin{cases} 0.5 & 0 < \alpha \leqslant 0.5 \\ 1 & 0.5 < \alpha \leqslant 1 \end{cases} \tag{35}$$

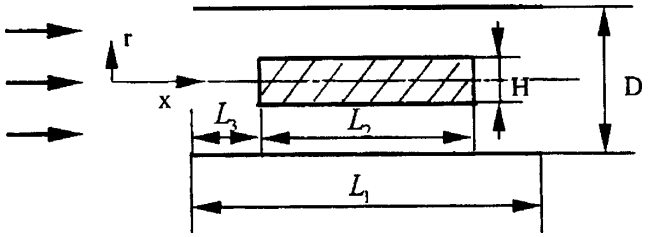

Fig. 19. Circular tube with coaxially inserted bar.

When underrelaxation of pressure is needed to ensure the convergence, β may take a value larger than 1.0. For cases where $\beta > 1$ is used special description will be provided.

3.3. Application examples of CLEAR algorithm

The CLEAR algorithm has been applied to solve six laminar fluid flow and heat transfer problems with available numerical solutions. Comparisons are made with the solutions from the SIMPLER algorithm under the same other conditions. The results of variation of iteration number and CPU time with the time step multiple E are shown in Figs. 10–15. From these results the superior performance of the CLEAR algorithm can be clearly observed.

4. Applications of the above achievements in the studies of heat transfer enhancement

Heat transfer enhancement is an everlasting subject of the international heat transfer community and many techniques have been developed in the past half century. Yet up to the end of last century, even for the single phase convective heat transfer, no unified theory could reveal the common essence of the heat transfer enhancement. In 1998 Guo and his coworkers [41,42] proposed a novel concept of enhancing convective heat transfer for parabolic flow. They transformed the convective term into the form of dot product of velocity and temperature gradient, and integrated the energy equation over the thermal boundary layer. They indicated that the reduction of the intersection angle between velocity and temperature gradient can effectively enhance the heat transfer. This concept has been extended by Tao et al. [43,44] to elliptic flow, and they pointed out that for fluid flow with Peclet number greater than 100, the integration of the convective term over the entire domain:

$$\mathrm{Int} = \int_{\Omega} \rho c_p \left(\vec{U} \cdot \nabla T\right) \mathrm{d}A = \int_{\Omega} \rho c_p \left|\vec{U}\right| |\nabla T| \cos\theta \, \mathrm{d}A \quad (36)$$

actually represents the convective heat transfer rate. Thus under some given condition, say, fixed flow rate and temperature difference between solid wall and the incoming fluid, the smaller the intersection angle the larger the heat transfer rate. This basic idea is called field synergy principle. For the simplicity of discussion, the intersection angle between velocity and temperature gradient will be call synergy angle hereafter.

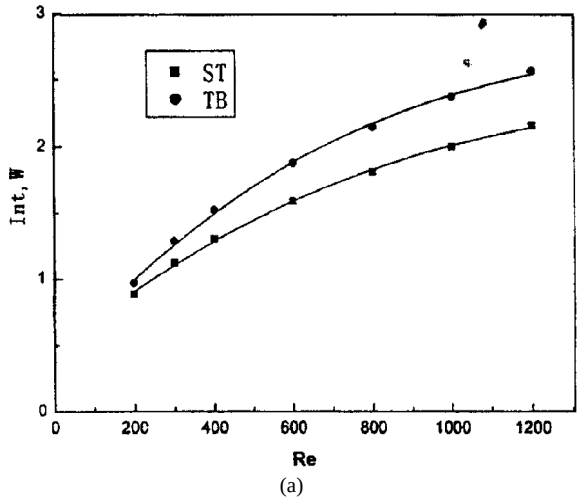

(a)

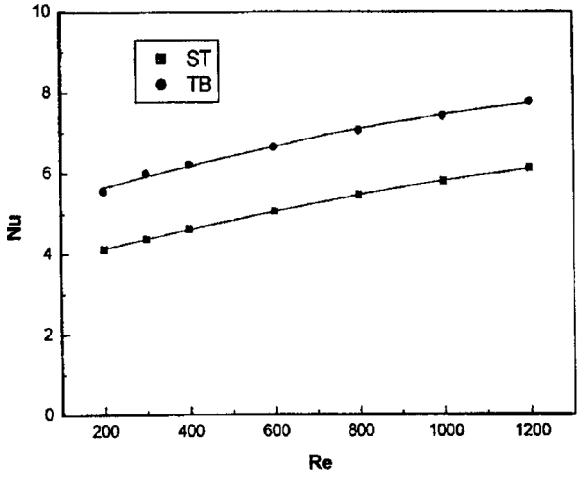

(b)

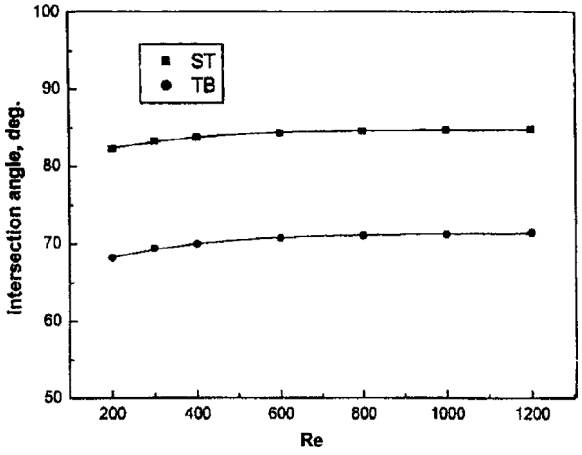

(c)

Fig. 20. Comparisons of tubes without bar (ST) and with bar (TB). (a) Integration vs. Re; (b) Nu vs. Re; (c) θ_m vs. Re.

By applying numerical methods described above, we have demonstrated that the field synergy principle (FSP) can

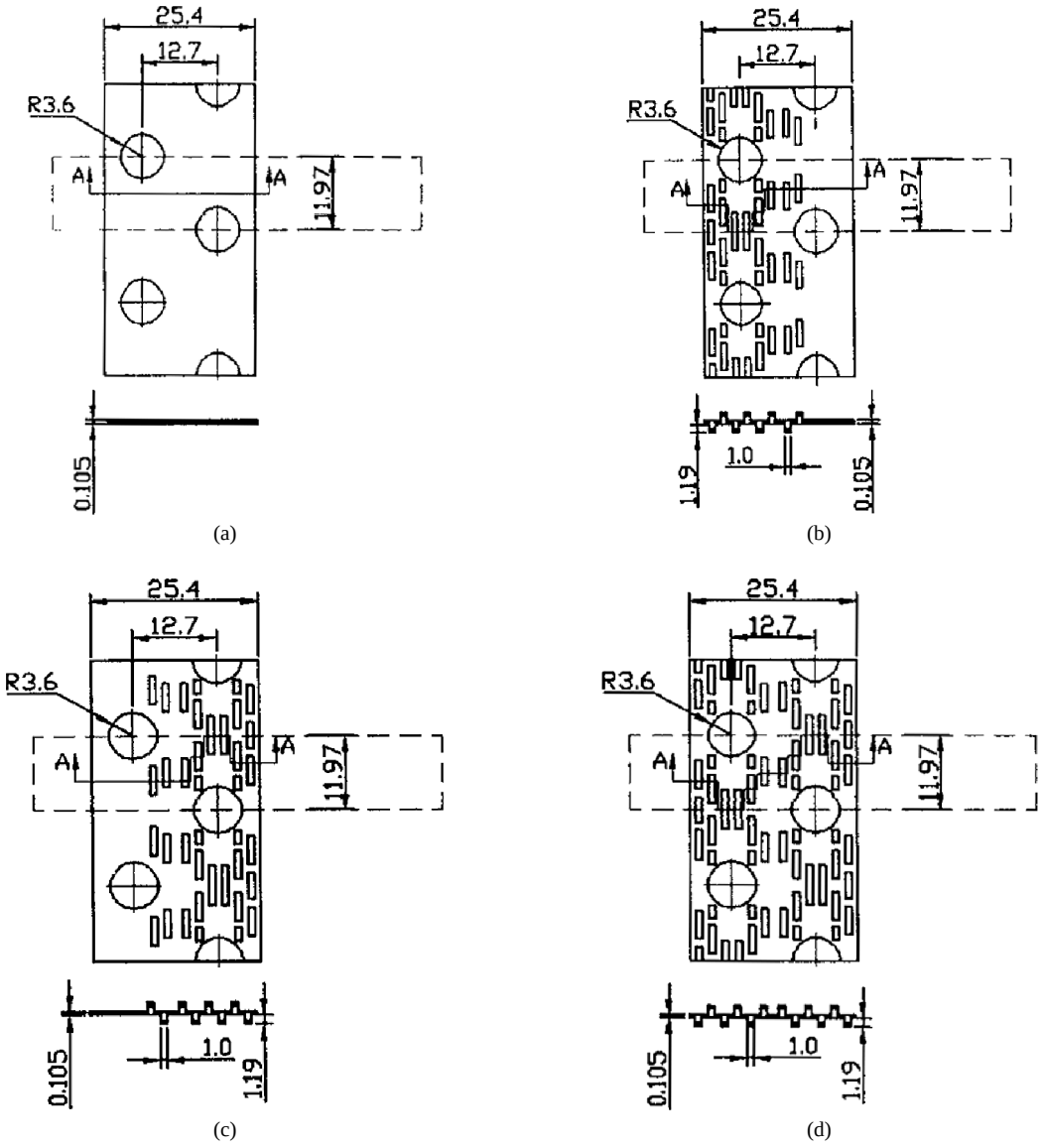

Fig. 21. The four types of slit arrangement. (a) Fin A; (b) Fin B; (c) Fin C; (d) Fin D.

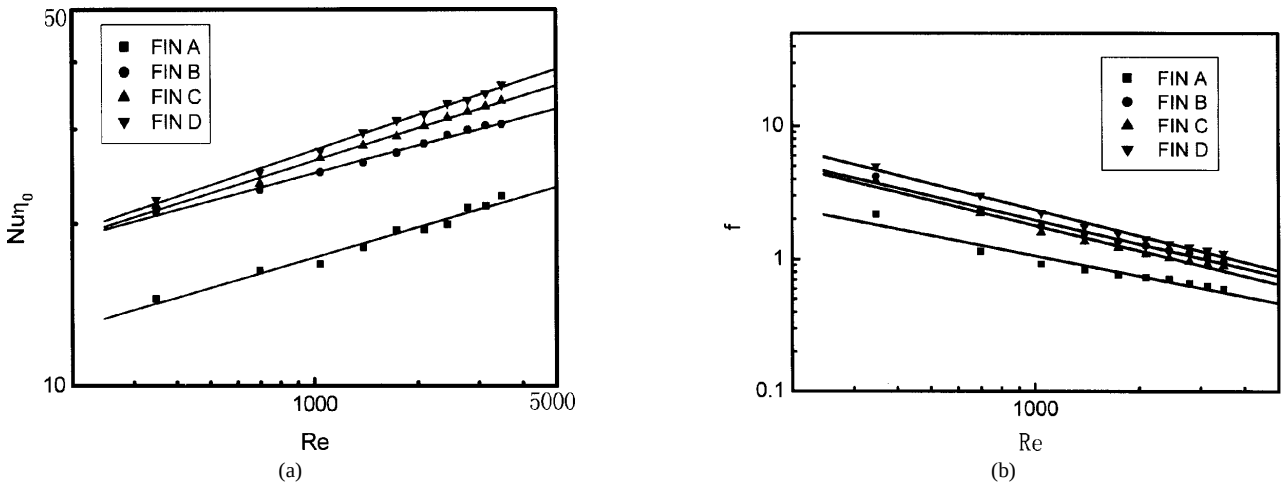

Fig. 22. Comparisons of the four slit arrangements. (a) Nu vs. Re; (b) f vs. Re.

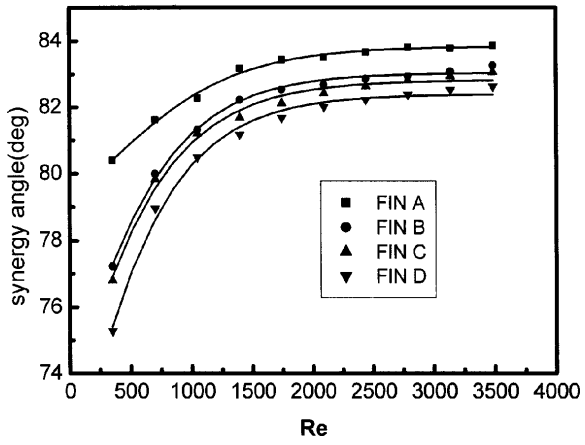

Fig. 23. Variations of intersection angle with Reynolds number.

unify the three existing explanations for enhancing convective heat transfer. Furthermore FSP is a powerful tool o develop new enhanced surfaces. These results are now briefly presented below.

4.1. Reducing the thermal boundary layer is equivalent to reducing synergy angle

Fig. 16 shows the numerical results for heat transfer over a flat plate with Reynolds number based on the plate length being 600. The ordinate represents the computed average synergy angle, local heat transfer coefficient and the value of Int at each cross section, with the streamwise coordinate being the abscissa. It can be seen that the decrease of the thermal boundary layer is equivalent to the reduction of the intersection angle between velocity and temperature gradient.

4.2. Increasing the interruption within fluid leads to deceasing the synergy angle

Fig. 17 shows a parallel plate channel with two-inserted blocks for enhancing convective heat transfer. Numerical results of Int, Nu and the average synergy angle are presented in Fig. 18. They definitely show that the increase of interruption within fluid is actually to decrease the intersection angle between velocity and temperature gradient.

4.3. Increasing the velocity gradient near solid wall results in the decrease of synergy angle

A model is set as shown in Fig. 19 to simulate the effect of increased velocity gradient near the solid wall under the same mass flow rate. The numerical results are presented in Fig. 20. For this case the Reynolds number definitions of the empty channel and the center-blocked channel are the same. Numerical simulation results reveal that the increase in the near wall velocity gradient also leads to the decrease in the intersection angle between the velocity and the temperature gradient.

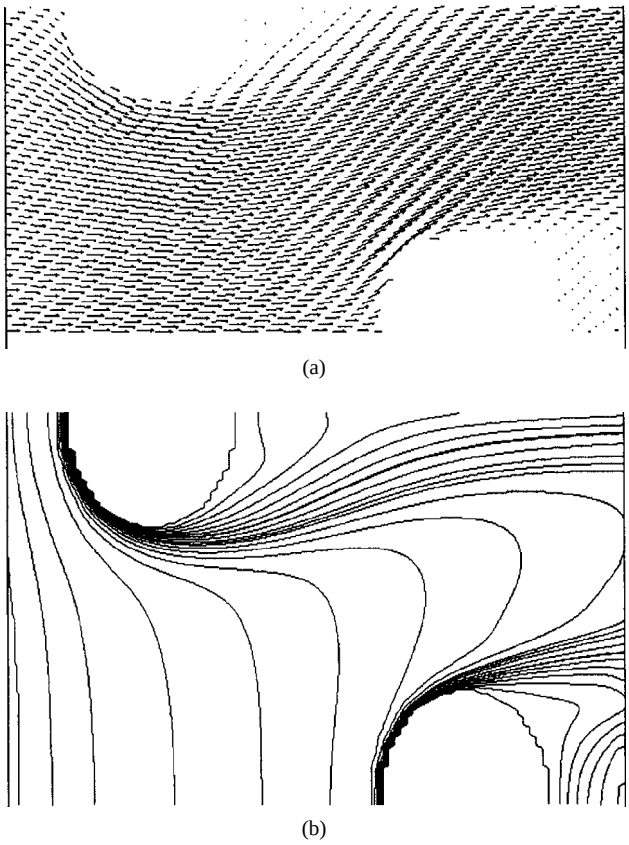

Fig. 24. Velocity and temperature fields in the middle plane between two adjacent fin surfaces: (a) Velocity field; (b) Isothermals.

4.4. FSP is a powerful tool in developing heat transfer enhanced surface

Numerical simulations were conducted for the four types of plate-fin and tube heat transfer surfaces shown in Fig. 21 [45]. Among the four surfaces, one is plain plate fin and the others are slotted fin surfaces. Fin B and fin C possess the same number of slits, but the positions of slits are different. In fin B the slits are mainly in the front part of the surface, while in fin C the slits are mainly in the rear part. The simulated results are presented in Figs. 22. It can be seen that fin C possesses superior performance than fin B. This finding is consistent with the experimental results provided by Kang and Kim [46].

From the average synergy angle presented in Fig. 23 it can be seen that the synergy of velocity and temperature gradient in fin C is better than that in fin B. In order to further reveal the reason, the velocity and temperature field of the middle plane between two adjacent plain plate fin surfaces (Fig. 24) are carefully examined, and following facts are found. In the rear part of the fin surface, the local velocity is almost parallel to local isothermal. This means that the local temperature gradient is almost normal to the velocity, indicating a bad synergy between the two vectors. Thus from the point view of FSP, it is this place that techniques should be adopted to enhance the heat transfer. The position of slits

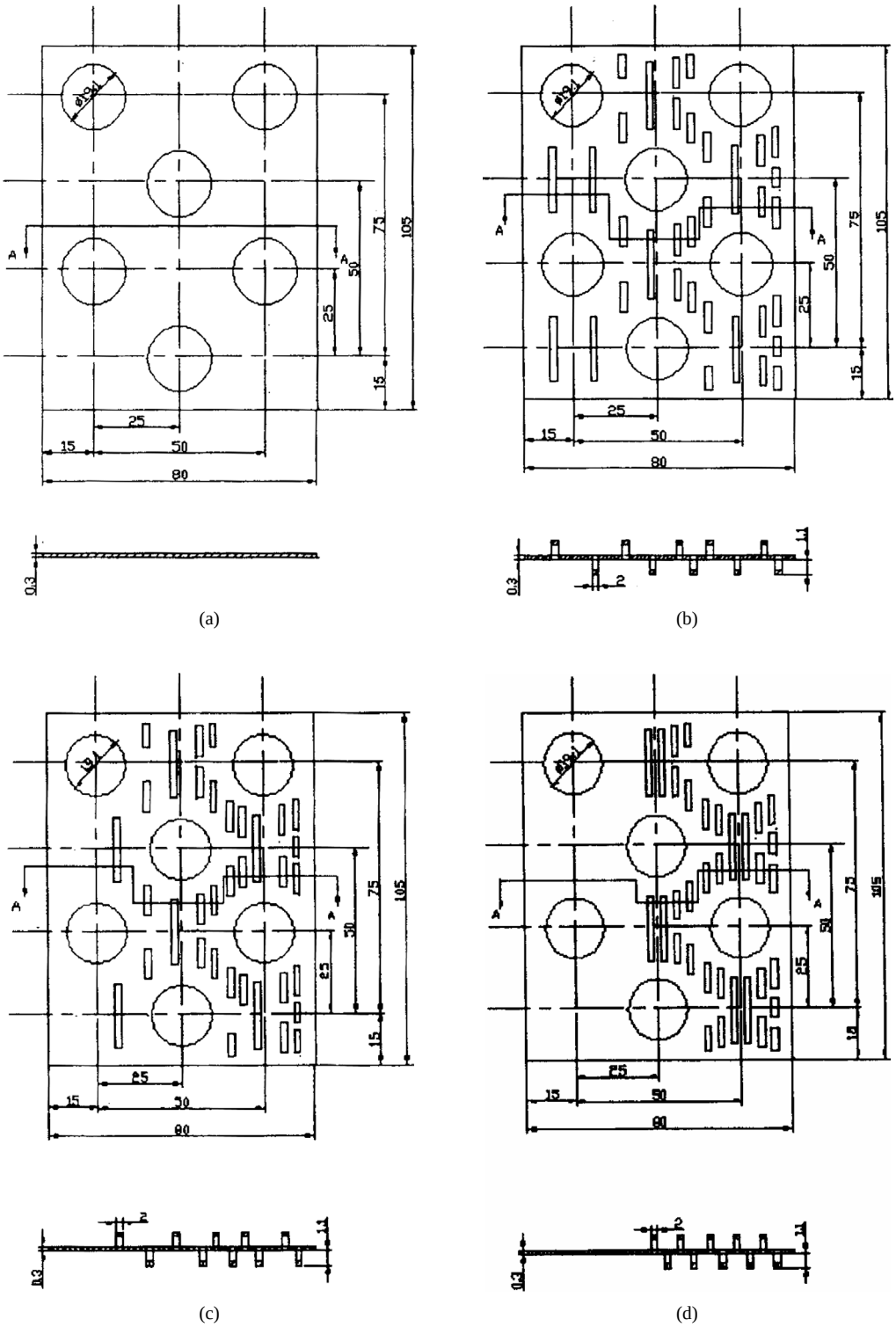

Fig. 25. Design for the optimum slit arrangement: (a) Plain plate fin; (b) Slit fin 1; (c) Slit fin 2; (d) Slit fin 3.

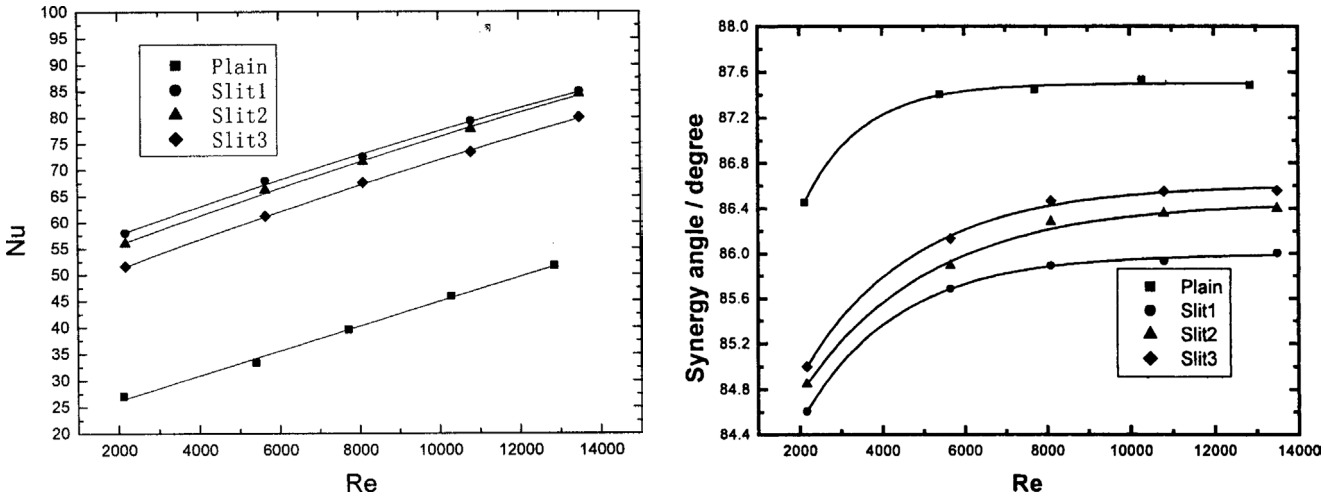

(a) (b)

Fig. 26. Comparison under identical flow rate: (a) *Nu* vs. *Re*; (b) Synergy angle vs. *Re*.

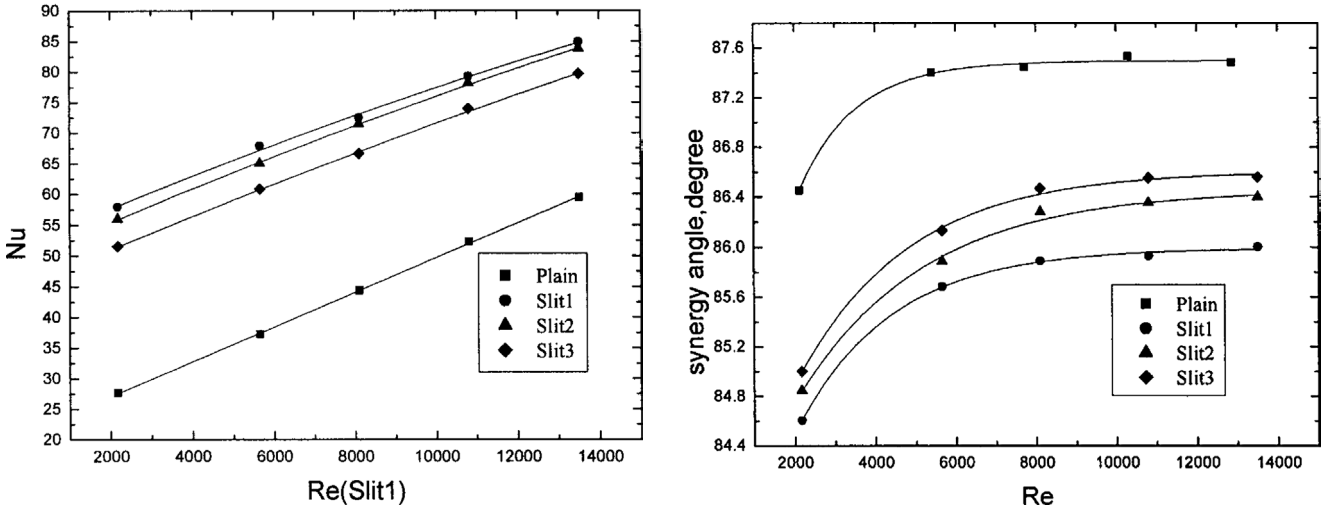

(a) (b)

Fig. 27. Comparison under identical pressure drop: (a) *Nu* vs. *Re* (Slit1); (b) Synergy angle vs. *Re* (Slit1).

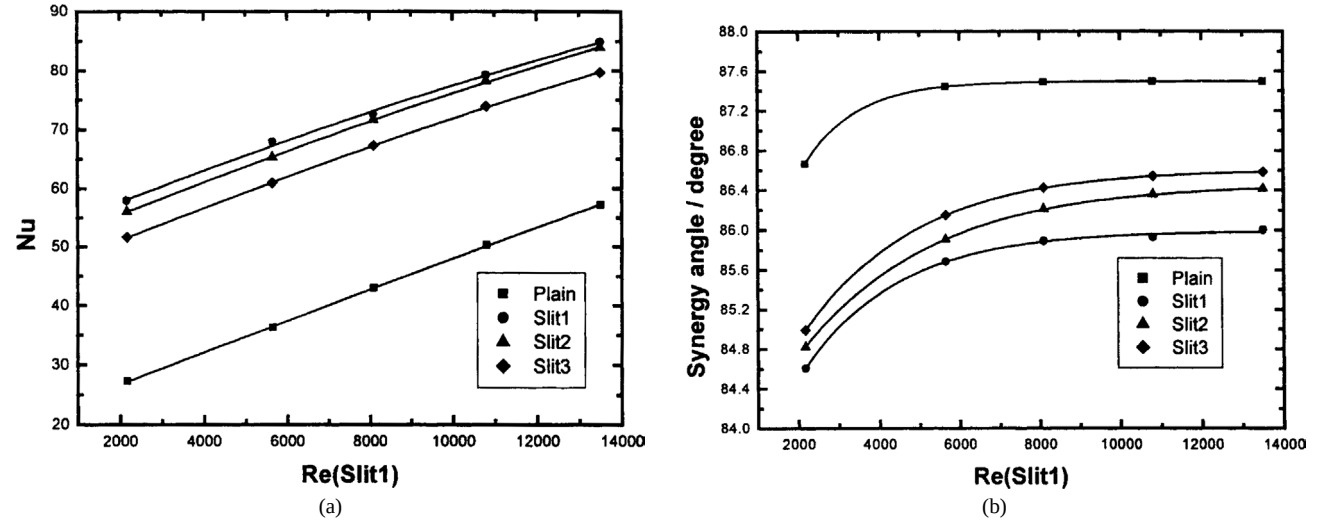

(a) (b)

Fig. 28. Comparison under identical pumping power: (a) *Nu* vs. *Re* (Slit1); (b) Synergy angle vs. *Re* (Slit1).

in fin C is consistent with this requirement, therefore fin C possesses a better performance than fin B. This gives us a useful hint: the slits of the slotted fin surface should be positioned in the fin surface according the rule of "front sparse and rear dense" [45,47].

The above rule for positioning slits was adopted to design an efficient slotted fin surface for an air intercooler. By preliminary computations to search for slit position pattern which possesses a smaller synergy angle, three position patterns were selected. They are shown in Fig. 25. Numerical simulation of heat transfer and flow filed are performed and the results are compared with the corresponding plain plate fin under three constraints: identical flow rate, identical pressure drop and identical pumping power. For all the three constraints, the three selected slotted fin surface have much better heat transfer performance, with slit 1 being the superior, followed by slit 2 and 3 in order. The heat transfer rate of slit 1 is 112 to 48% higher than that of the plain plate fin surface. And slit 1 always superior to slit 3 by about 10 percent in heat transfer rate, and slit 2 is somewhat in between. The synergy angle of the three slotted fin and the corresponding plain plate fin are presented in Figs. 26–28. The results are in good consistency with FSP.

5. Conclusions

Scheme and algorithm are the two major numerical issues in the solution of incompressible flow by the finite volume approach. Significant improvements are made during the past five years, making the approach more attractive and powerful for heat transfer engineering application. These include the SGSD scheme which is absolutely stable and possesses at least second-order accuracy, and the CLEAR algorithm which is fully implicit and can appreciably accelerate the convergence rate by a slight change of the existing code using SIMPLER. It is expected that both SGSD and CLEAR will be widely adopted in the solutions of fluid flow and heat transfer problems.

Numerical experiments by the finite volume approach incorporated by the proposed scheme and algorithm are conducted to demonstrate that the field synergy principle can unify the three existing mechanisms of enhancing convective heat transfer. An example is provided to show that the field synergy principle is a very powerful tool in the designing of new enhancement surface.

Acknowledgements

The authors' papers cited here are supported by the following Chinese Foundations:

The National Natural Science Foundation of China (Grant No. 50476046, 50236010);

The National Science Fund for Distinguished Young Scholars from the National Natural Science Foundation of China (No. 50425620);

The Research Fund for the Doctoral Program of Higher Education (RFDP20030698015);

The National Key Project of Fundamental R & D of China (Grant No. 2000026303).

References

[1] W.Q. Tao, E.M. Sparrow, The transportive property and convective numerical stability of the steady state convection–diffusion difference equation, Numer. Heat Transfer 11 (1987) 491–497.
[2] S.V. Patankar, Numerical Heat Transfer and Fluid Flow, McGraw-Hill, New York, 1980.
[3] P.M. Gresho, R.L. Lee, Don't suppress the wiggles—they are telling you something!, Comput. Fluids 9 (1981) 223–251.
[4] B.P. Leonard, A survey of finite differences with upwinding for numerical modeling of the incompressible convective diffusion equation, in: C. Taylor, K. Morgan (Eds.), Computational Techniques in Transient and Turbulent Flows, Pineridge Press, Swansea, 1981.
[5] B. Yu, W.Q. Tao, D.S. Zhang, Q.W. Wang, Discussion on numerical stability and boundedness of convective discretized scheme, Numer. Heat Transfer B Fund. 40 (2001) 343–365.
[6] Z.Y. Li, T.C. Hung, W.Q. Tao, Numerical simulation of heat transfer at an array of co-planar slat-like surfaces oriented normal to a forced convection flow, Internat. J. Comput. Appl. Technol. 13 (2000) 285–294.
[7] S.V. Patankar, Recent advances in computational heat transfer, ASME J. Heat Transfer 110 (1988) 1037–1045.
[8] Z.Y. Li, W.Q. Tao, A new stability-guaranteed second-order difference scheme, Numer. Heat Transfer B 42 (2002) 349–365.
[9] M.J. Ni, W.Q. Tao, S.J. Wang, Stability-controllable second-order difference scheme for convection term, J. Thermal Sci. 7 (1998) 119–130.
[10] U. Ghia, K.N. Ghia, C.T. Shin, High resolution of incompressible flow using the Navier–Stokes equations and a multigrid method, J. Comput. Phys. 48 (1982) 387–441.
[11] P.H. Gaskell, A.K.C. Lau, Curvature-compensated convective transport: SMART, a new boundedness-preserving transport algorithm, Internat. J. Numer. Methods Fluids 8 (1988) 617–641.
[12] S.K. Choi, H.Y. Nam, M. Cho, Evaluation of a higher order bounded convection scheme: three-dimensional numerical experiment, Numer. Heat Transfer B 28 (1995) 23–38.
[13] J. Zhu, W. Rodi, A low-dispersion and bounded convection scheme, Comput. Methods Appl. Mech. Engrg. 29 (1991) 87–96.
[14] J.J. Wei, B. Yu, W.Q. Tao, Y. Kawaguchi, H.S. Wang, A new high-order accurate and bounded scheme for incompressible flow, Numer. Heat Transfer B 43 (2003) 19–41.
[15] P.L. Hou, M.Z. Yu, W.O. Tao, Refinement of the convective boundedness criterion of Gaskell and Lau, Engineering Comput. 20 (2003) 1023–1043.
[16] B.P. Leonard, The EULER-QUICK code, in: C. Taylor, K. Morgan (Eds.), Numerical Methods in Laminar and Turbulent Flows, Pineridge Press, Swansea, 1983.
[17] J. Zhu, A low-diffusive and oscillation-free convective scheme, Comm. Appl. Mech. Engrg. 7 (1991) 225–232.
[18] B.V. Leer, Towards the ultimate conservation difference scheme. V. A second order sequel to Godunov's method, J. Comput. Phys. 23 (1977) 101–136.
[19] S.R. Chakravarthy, S. Osher, High resolution of the OSHER upwind scheme for the Euler equations, AIAA Paper, 83-1943, 1983.
[20] M.S. Darwish, A new high resolution scheme based on the normalized variable formulation, Numer. Heat Transfer B 24 (1993) 353–371.

[21] B. Song, G.R. Liu, K.Y. Lam, R.S. Amano, On a higher-order discretization scheme, Internat. J. Numer. Methods Fluids 32 (2000) 881–897.
[22] S.V. Patankar, D.B. Spalding, A calculation procedure for heat, mass and momentum transfer in three-dimensional parabolic flows, Internat. J. Heat Mass Transfer 15 (1972) 1787–1806.
[23] S.V. Patankar, A calculation procedure for two-dimensional elliptic situations, Numer. Heat Transfer 4 (1981) 409–425.
[24] J.P. van Doormaal, G.D. Raithby, Enhancement of SIMPLE method for predicting incompressible fluid flows, Numer. Heat Transfer 7 (1984) 147–163.
[25] J.P. van Doormaal, G.D. Raithby, An evaluation of the segregated approach for predicting incompressible fluid flow, ASME Paper 85-HT-9, 1985.
[26] G.D. Raithby, G.E. Schneider, Elliptic system: finite difference method II, in: W.J. Minkowycz, E.M. Sparrow, R.H. Pletcher, G.E. Schneider (Eds.), Handbook of Numerical Heat Transfer, Wiley, New York, 1988, pp. 241–289.
[27] R.I. Issa, Solution of implicitly discretized fluid flow equation by operator-splitting, J. Comput. Phys. 62 (1985) 40–65.
[28] S.D. Connell, P. Stow, The pressure correction methods, Comput. Fluids 14 (1986) 1–10.
[29] A.U. Chatwani, A. Turan, Improved pressure-velocity coupling algorithm based on global residual norm, Numer. Heat Transfer B 20 (1991) 115–123.
[30] L.S. Lee, R.Y. Tzong, Artificial pressure for pressure linked equation, Internat. J. Heat Mass Transfer 35 (1992) 2705–2716.
[31] R.H. Yen, C.H. Liu, Enhancement of the SIMPLE algorithm by an additional explicit corrector step, Numer. Heat Transfer B 24 (1993) 127–141.
[32] X. Wen, D.B. Ingham, A new method for accelerating the rate of convergence of the SIMPLE-like algorithm, Internat. J. Numer. Methods Fluids 17 (1993) 385–400.
[33] T. Gjesdal, M.E.H. Lossius, Comparison of pressure correction smoothers for multigrid solution of incompressible flow, Internat. J. Numer. Methods Fluids 25 (1997) 393–405.
[34] Y. Sheng, M. Shoukri, G. Sheng, P. Wood, A modification to the SIMPLE method for buoyancy-driven flows, Numer. Heat Transfer B 33 (1998) 65–78.
[35] B. Yu, H. Ozoe, W.Q. Tao, A modified pressure-correction scheme for the SIMPLER method, MSIMPLER, Numer. Heat Transfer B 39 (2001) 439–449.
[36] F. Moukalled, M. Darwish, A unified formulation of the segregated class of algorithm for fluid flow at all speeds, Numer. Heat Transfer B 37 (2000) 103–139.
[37] E. Blosch, W. Shyy, The role of mass conservation in pressure-based algorithms, Numer. Heat Transfer B 24 (1993) 415–429.
[38] W.Q. Tao, Z.G. Qu, Y.L. Hr, A novel segregated algorithm for incompressible flow and heat transfer problems—CLEAR (Coupled Equations Algorithm Revised) Part 1: Mathematical formulation and solution procedure, Numer. Heat Transfer B 45 (2004) 1–18.
[39] W.Q. Tao, Z.G. Qu, Y.L. Hr, A novel segregated algorithm for incompressible flow and heat transfer problems—CLEAR (Coupled Equations Algorithm Revised) Part 2: Application examples, Numer. Heat Transfer B 45 (2004) 19–48.
[40] W.Q. Tao, Numerical Heat Transfer, second ed., Xi'an Jiaotong University Press, Xi'an, 2001.
[41] Z.Y. Guo, D.Y. Li, B.X. Wang, A novel concept for convective heat transfer enhancement, Internat. J. Heat Mass Transfer 41 (1998) 2221–2225.
[42] S. Wang, Z.X. Li, Z.Y. Guo, Novel concept and devices of heat transfer augmentation, in: Proceedings of 11th International Conference of Heat Transfer, vol. 5, Taylor & Francis, 1998, pp. 405–408.
[43] W.Q. Tao, Z.Y. Guo, B.X. Wang, Field synergy principle for enhancing convective heat transfer—its extension and numerical verifications, Internat. J. Heat Mass Transfer 45 (2002) 3849–3856.
[44] W.Q. Tao, Y.L. He, Q.W. Wang, Z.G. Qu, F.Q. Song, A unified analysis on enhancing convective heat transfer with field synergy principle, Internat. J. Heat Mass Transfer 45 (2002) 4871–4879.
[45] Z.G. Qu, Y.L. He, W.Q. Tao, 3D Numerical simulation on laminar heat transfer and fluid flow characteristics of strip fin surface with X-arrangement of strips, ASME J. Heat Transfer 126 (2004) 697–707.
[46] H.C. Kang, M.H. Kim, Effect of strip location on the air-side pressure drop and heat transfer in strip fin-and-tube heat exchanger, Internat. J. Refrig. 22 (1999) 302–312.
[47] Y.P. Cheng, Z.G. Qu, W.Q. Tao, Y.L. He, Numerical design of efficient slotted fin surface based on the field synergy principle, Numer. Heat Transfer A 45 (2004) 517–538.